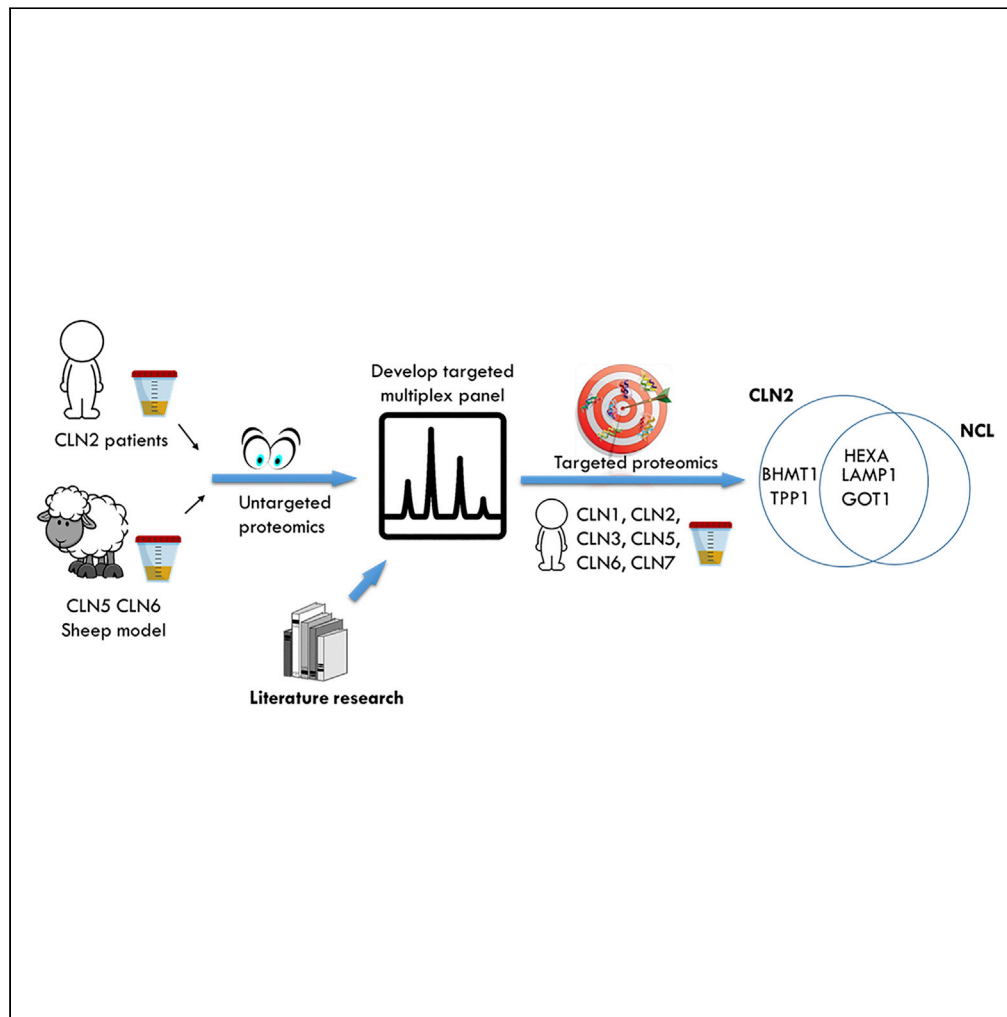


Article

Urine proteomics analysis of patients with neuronal ceroid lipofuscinoses



Katharina Iwan,
Robert Clayton,
Philippa Mills, ...,
David N. Palmer,
Kevin Mills, Wendy
E. Heywood

wendy.heywood@ucl.ac.uk

HIGHLIGHTS

The urine proteome is altered in humans and animals with NCL

Hexosaminidase A and LAMP1 are increased in patients with NCL

Betaine-homocysteine S-methyltransferase 1 is elevated in CLN2 patients

Proteins altered in CLN5 and CLN6 sheep models are not affected in humans

Iwan et al., iScience 24, 102020
February 19, 2021 © 2020 The Authors.
<https://doi.org/10.1016/j.isci.2020.102020>



Article

Urine proteomics analysis of patients with neuronal ceroid lipofuscinoses

Katharina Iwan,¹ Robert Clayton,¹ Philippa Mills,^{1,2} Barbara Csanyi,³ Paul Gissen,^{1,2,3} Sara E. Mole,^{1,4} David N. Palmer,⁵ Kevin Mills,^{1,2} and Wendy E. Heywood^{1,2,6,*}

SUMMARY

The neuronal ceroid lipofuscinoses (NCL) are a group of 13 rare neurodegenerative disorders characterized by accumulation of cellular storage bodies. There are few therapeutic options, and existing tests do not monitor disease progression and treatment response. However, urine biomarkers could address this need. Proteomic analysis of CLN2 patient urine revealed activation of immune response pathways and pathways associated with the unfolded protein response. Analysis of CLN5 and CLN6 sheep model urine showed subtle changes. To confirm and investigate the relevance of candidate biomarkers a targeted LC-MS/MS proteomic assay was created. We applied this assay to additional CLN2 samples as well as other patients with NCL (CLN1, CLN3, CLN5, CLN6, and CLN7) and demonstrated that hexosaminidase-A, aspartate aminotransferase-1, and LAMP1 are increased in NCL samples and betaine-homocysteine S-methyltransferase-1 was specifically increased in patients with CLN2. These proteins could be used to monitor the effectiveness of future therapies aimed at treating systemic NCL disease.

INTRODUCTION

The neuronal ceroid lipofuscinoses (NCLs, Batten disease) are a heterogeneous group of rare neurodegenerative diseases that present mainly in childhood and as a combined group represent the most common cause of childhood neurodegeneration and dementia. The group share phenotypic characteristics including seizures, visual loss, loss of motor skills, and cognitive function resulting in premature death, but each subtype is a distinct genetic entity with unique pathophysiological characteristics (Kohlschütter et al., 2019). Brain pathology reveals a massive loss of neurons, and most cells throughout the body contain lysosome-derived fluorescent storage bodies, the main component of which is the c subunit of mitochondrial ATP synthase or Saposins A and D (Palmer, 2015). So far, at least 13 genes have been identified that lead to NCL (CLN1–8, 10–14) (Butz et al., 2020; Williams and Mole, 2012). Of all the NCLs, CLN2 disease is one of the most commonly reported with an incidence in Europe varying between 0.15 and 0.78 per 100,000 live births. Autosomal recessive mutations in the *TPP1* gene lead to loss or deficiency of the lysosomal enzyme tripeptidyl peptidase 1 (TPP1). TPP1 is a lysosomal serine protease that cleaves tripeptides from the N termini of small polypeptides during protein degradation inside the lysosomes (Golabek et al., 2003; Wlodawer et al., 2003). Five other NCLs occur due to a lack or defect of lysosomal-associated proteins, namely, palmitoyl protein thioesterase 1 (PPT1) in CLN1, CLN5 in CLN5, cathepsin D (CTSD) in CLN10, progranulin in CLN11, and cathepsin F (CTSF) in CLN13 diseases. Other NCL forms resulting from missing or defective lysosomal membrane proteins are CLN3, CLN7/MFSD8, and CLN12/ATP13A2 diseases. CLN6 and CLN8 diseases result from deficiencies of endoplasmic reticulum (ER) membrane proteins CLN6 and CLN8 (di Ronza et al., 2018; Mole et al., 2004). The very rare CLN4 disease results from defects in a chaperone protein DNAJC5 (Henderson et al., 2016), and CLN14 disease results from defects in the plasma membrane potassium channel KCTD7 gene (Staropoli et al., 2012).

To date, the only clinically approved treatment that has slowed disease progression is Brineura (cerliponase alfa) for CLN2 disease. This TPP1 enzyme replacement therapy (ERT) is delivered intra-cerebroventricularly into the brain ventricles of patients every fortnight (Schulz et al., 2018). Other treatment approaches in development for NCL include gene therapy, various small molecules, and the administration of immunosuppressive drugs to prevent neuroinflammation (Kohlschütter et al., 2019; Mole et al., 2019). Initial animal studies

¹Inborn Errors of Metabolism Section, Genetics & Genomic Medicine Unit, Great Ormond Street Institute of Child Health, University College London, 30 Guilford Street, London WC1N 1EH, UK

²NIHR Great Ormond Street Hospital Biomedical Research Centre, University College London, London, UK

³Great Ormond Street Hospital for Children, London, UK

⁴MRC Laboratory for Molecular Cell Biology, University College London, London, UK

⁵Department of Molecular Biosciences, Agriculture and Life Sciences Faculty, University Lincoln 7647, Canterbury, New Zealand

⁶Lead contact

*Correspondence:

wendy.heywood@ucl.ac.uk
<https://doi.org/10.1016/j.isci.2020.102020>



have shown promising results for an ERT with the recombinant proenzyme PPT1 for patients with CLN1 disease (Lu et al., 2015; Hu et al., 2012). ERT administered directly into the brain still cannot prevent loss of vision, hence additional intraocular/intravitreal treatment is necessary (Katz et al., 2014; Tracy et al., 2016; Whiting et al., 2014; Griffey et al., 2005; Mole et al., 2019). Clinical trials for gene therapy for patients with CLN2, CLN3, and CLN6 disease have begun (Liu et al., 2020; Kohlschütter et al., 2019), and promising data for an early clinical trial for CLN2 disease suggest an attenuation of neurological impairment. So far, preclinical and clinical studies indicate that a single treatment strategy will not suffice, as therapeutic strategies have to target the brain, the retina, and peripheral organs (Kohlschütter et al., 2019; Mole et al., 2019).

Clinical diagnoses of specific NCL forms are still challenging with investigations mainly only being conducted after NCL disease is suspected after the first symptoms are detected. Early or new-born diagnosis is crucial if a small therapeutic window exists where successful interventions can more effectively prevent or slow the neurological disease progression. Diagnosis of NCL used to require microscopic analysis of storage material using a skin biopsy. Nowadays, genetic testing and enzyme activity assays are the methods of choice. Although genetic tests can be used to diagnose the NCL form, they cannot monitor disease progression or response to treatments. Typically disease progression is determined using baseline clinical scores like the Unified Batten Disease Rating Scale (UBDRS) (de Bleeck et al., 2013; Adams and Mink, 2013), the Weill Cornell CNS scale, and the Hamburg CLN2 scale to quantify seizures, loss of language, motor skills, and visual function. To accompany the clinical presentation, assessing what is happening at the molecular level will be crucial in monitoring early stages of disease and for preclinical studies or ongoing clinical trials. Robust molecular biomarkers are therefore needed to monitor even subtle changes in physiological or pathological disease progression.

Various biomarker studies in patients with different NCLs have previously been conducted to identify possible biomarkers of disease progression. Using proteomics, Sleat et al. (2017) investigated cerebrospinal fluid (CSF) and postmortem brain samples of patients with CLN1, CLN2, and CLN3 disease. Initially they investigated lysosomal proteins, i.e., TPP1, beta-hexosaminidase subunit alpha (HEXA), and cathepsins, as they are known to be altered in many lysosomal storage disorders (Sleat et al., 2017). Other studies analyzed CSF from patients with CLN2 disease and identified metabolites that correlated to disease severity scores (Sindelar et al., 2018). Urine is a highly desirable body fluid for biomarker analysis because collection is non-invasive, feasible in relatively large volumes, and at frequent intervals; because it is inexpensive to preserve; and, due to its high urea content, urine proteins are considered more stable than serum or plasma proteins. The urinary proteins present derive from glomerular filtrations of plasma, renal tubule excretion, and urogenital tract secretion, with fluctuations representing normal physiological changes as well as pathological changes due to renal or systemic disease (Harpole et al., 2016; Kalantari et al., 2015).

One of the greatest challenges in biomarker research in rare diseases is accessing enough samples for a viable study. Often researchers turn to animal or cell models to address this. One such model is the slime mold *Dictyostelium*, which has revealed how secretion is impaired in NCL (Huber et al., 2014; Huber, 2020). Proteins observed to be altered in *Dictyostelium* were also observed to be altered in human patient tissues (Sleat et al., 2017).

Experimental design

We have used both human and animal models in a two-phase proteomic strategy to identify proteins altered in patients with NCL.

Phase 1 the “discovery” step is an unbiased eyes-open approach that uses label-free proteomic profiling to study urine from patients with CLN2 disease and CLN5 and CLN6 disease sheep models. The technology is semi-quantitative and lengthy, therefore small sample cohorts are analyzed using this approach.

Phase 2 involves a targeted analysis using multiple reaction monitoring mass spectrometry coupled with liquid chromatography (LC-MS). A candidate biomarker peptide(s) is accurately quantitated using this technique, and multiple peptides can be measured in one analysis, therefore creating a multiplex approach. Proteins of interest identified from the phase 1 profiling analysis are considered as potential biomarker candidates for corresponding CLN2, CLN5, and CLN6 diseases in human patients. As additional biomarkers can be included we also selected peptides from other biomarker candidates described in previous NCL omics studies (Sleat et al., 2017, 2019) to confirm these in our analyses. Using the targeted

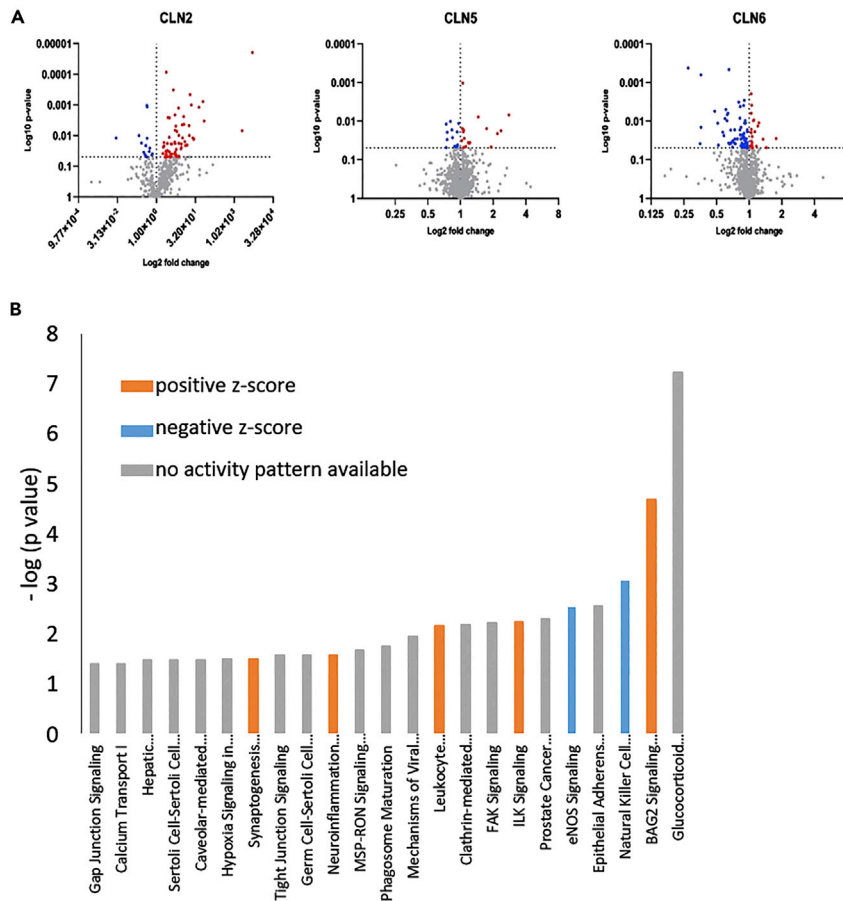


Figure 1. Label-free proteomic analysis of urine from CLN2 patients and CLN5 and CLN6 sheep models

(A) Volcano plots summarizing the proteomic data. Proteins highlighted in red are significantly upregulated, proteins highlighted in blue are downregulated, whereas the proteins in gray are not significantly changed (p (ANOVA) < 0.05). (B) Summary of the affected pathways in CLN2 patient urine as determined by Ingenuity Pathway Analysis (Qiagen). This shows which cellular pathways are altered significantly in urine of patients with CLN2 disease compared with healthy controls. Only proteins that were significantly (p (ANOVA) < 0.05) changed with a fold change >2 or < -2 were used for this analysis. The y axis depicts how significantly changed a pathway is in a negative logarithmic scale of the p values. The cutoff is 1.3 as this is the equivalent to a p value of 0.05. The activity pattern is color coded: bars in gray indicate it is unknown if the pathway is activated or inactivated, bars in blue label negative z values and therefore inhibited pathways, whereas positive z values and therefore activated pathways are highlighted in orange.

multiplex assay we applied this to a larger separate cohort of CLN2 disease patient samples and patient samples with CLN5 and CLN6 disease to confirm phase 1 findings. To see if the biomarkers may be specific for the NCL type we also included analyses of the NCL diseases CLN1, CLN3, and CLN7.

RESULTS

Phase 1: Proteomic screening of urine from human and animal models of NCL disease identify candidate biomarkers and affected pathways

Untargeted proteomic analyses of two patients with CLN2 disease and comparison with four age-matched healthy control samples demonstrated an increase in 61 proteins (p value < 0.05 with a normalized fold change >2) and 11 proteins with reduced levels (p value < 0.05 and normalized fold change < -2, [Table S1](#)). Additionally, proteomic analyses of urine from 3 CLN5-affected sheep and 13 CLN6-affected sheep were compared with seven normal control sheep ([Tables S2 and S3](#)). The volcano plot in [Figure 1A](#) summarizes the alterations found in the urinary proteome of patients with CLN2 disease and the CLN5 and CLN6 sheep models. The CLN5 profile shows the least number of significant proteins altered among the three NCL urine profiles.

To gain some insight into the effects of CLN2 disease on biological pathways an Ingenuity Pathway Analysis (IPA, QIAGEN Inc., <https://www.qiagenbioinformatics.com/products/ingenuitypathway-analysis>) was conducted on the differentially expressed proteins (Figure 1B). Pathways showing no activity pattern ($z = 0$) were omitted. The most significantly activated pathway is the BAG2 signaling pathway, with altered levels of proteins Annexin A2, Heat shock 70 kDa protein 1A/B, and Heat shock 70 kDa proteins 2 and 8. Interestingly, the neuroinflammation signaling pathway and the synaptogenesis signaling pathway are both significantly activated, whereas the natural killer cell signaling pathway is inhibited. A functional enrichment gene ontology analysis for cellular components (CC) performed using the DAVID bioinformatics website (Huang et al., 2008, 2009) confirmed that the differentially expressed proteins detected in the urine proteome were derived from the lysosomal lumen and the lysosome (Table S4). The proteins affected primarily in patients with CLN2 disease were GOT1 aspartate aminotransferase and FMO3 dimethylaniline monooxygenase, which were absent in controls. IPA analysis was also performed on the CLN5 and CLN6 disease sheep urine proteomic data (Figure S1).

The CLN5 and CLN6 sheep datasets had one significant pathway in common, the LXR/RXR activation pathway. Interestingly, the ER stress response pathway was affected in the CLN6 sheep, as was an unfolded protein response pathway and pathways associated with the immune response. In CLN5-affected sheep, however, there were greater effects on pathways associated with carbohydrate metabolism. Significant proteins affected in CLN5 sheep urine showed small fold changes. Only one protein, beta enolase, a muscle-specific form of enolase, was increased more than 2-fold. The number of significantly affected proteins in CLN6 sheep urine was greater than that seen in CLN5 urine, whereas the fold changes were similarly small. The most affected protein, ERICH6B, glutamate-rich protein 6B of unknown function, showed a >2-fold reduction in amount.

Phase 2: confirmation of human and animal model discovery targets in an extended NCL patient cohort

A multiplexed, targeted proteomic assay was developed to confirm if the changes in pathways and protein levels observed in the proteomic profiling analyses could be detected in a separate and larger number of 9 CLN2 patient samples and 13 controls. A selection of proteins from the sheep proteomic analyses was also included to see if they were relevant in human CLN5 ($n = 2$) and CLN6 ($n = 2$) urine. Candidate selection criteria are given in methods, and the proteins included in the multiplex assay are shown in Table 1. Urine from patients with other NCL disorders, CLN1 ($n = 2$), CLN3 ($n = 1$), and CLN7 ($n = 1$), was also analyzed to determine whether our initial discovery findings were specific to CLN2, CLN5, and CLN6 or if similar findings could be attributed to all NCL disorders. Further sample details are given in Table S7 in methods.

Multivariate-principal component analysis (PCA) was performed to determine if the proteins in the biomarker panel are able to collectively distinguish between the control and patient samples. Figure 2 shows a PCA plot of all samples apart from one omitted outlier (patient CLN2 (4)-post). The first two components ($t[1]$ and $t[2]$) explain 27% and 19.2% of the variance in urine. The variation within the dataset roughly separates the patient samples from the control samples. Some patient samples were present within the cluster of control samples (particularly CLN6 and CLN7) indicating they have a normal urine profile. The other NCL urines show a dispersed profile indicating a large degree of variation, which is away from the cluster of control samples. This indicates that these NCL urine profiles are abnormal compared to controls.

The loading plot of the multivariate analysis indicated that lysosome-associated membrane glycoprotein 1 (LAMP1), peptidyl-glycine alpha-amidating monooxygenase (PAM), and aspartate aminotransferase, cytoplasmic (GOT1) are the biggest drivers of the difference observed in the two clusters, i.e., controls and patients.

Proteins affected in CLN2 disease: Figure 3A shows univariate analysis of proteins in CLN2 patient urine compared with age- and sex-matched controls. Peptide ratios representative of betaine-homocysteine S-methyltransferase 1 (BHMT1), LAMP1, and TPP1 were significantly altered in CLN2 disease samples. As patients with CLN2 disease have mutations in the *TPP1* gene this result was expected, with the level of TPP1 approaching zero. Conversely, levels of urinary BHMT1 and LAMP1 were increased, on average 17.8- and 3.4-fold, respectively, compared with the control samples. Two of these three proteins, TPP1 and BHMT1, are specific for CLN2 (Figure 3B): BHMT1 is increased 16-fold and TPP1 is decreased up to

Table 1. Multiplex panel of proteins listed with their corresponding gene names and cellular location

Gene	CLN2 patients (label-free proteomics)	Location
GOT1	Aspartate aminotransferase, cytoplasmic	Cytoplasm
CTSH	Pro-cathepsin H	Lysosome
PEBP1	Phosphatidylethanolamine-binding protein 1	Cytoplasm
CTSZ	Cathepsin Z	Lysosome
AKT1	RAC-alpha serine/threonine-protein kinase	Nucleosome/cytoplasm
GALNS	N-acetylgalactosamine-6-sulfatase	Lysosome
BHMT1	Betaine-homocysteine S-methyltransferase 1	Cytoplasm
LAMP1	Lysosome-associated membrane glycoprotein 1	Lysosome/endosome
HEXA	Beta-hexosaminidase subunit alpha	Lysosome

Literature research NCL biomarker

CTSL1	Cathepsin L1*	Lysosome
TPP1	Tripeptidyl-peptidase 1*	Lysosome
PAM	Peptidyl-glycine alpha-amidating monooxygenase [#]	Secreted
GM2A	Ganglioside GM2 activator ^o	Secreted
NAGA	Alpha-N-acetylgalactosaminidase*	Lysosome

CLN5 and CLN6 sheep (label free proteomics)

LEAP2	Liver-expressed antimicrobial peptide 2	Secreted
DSC2	Desmocollin-2	Cell membrane
SCGN	Secretagogin	Secreted
LAMP2	Lysosome-associated membrane glycoprotein 2	Lysosome/endosome

CLN6 sheep (label-free proteomics)

CTSB	Cathepsin B	Lysosome
------	-------------	----------

The list is subdivided by the origin of the proteins, i.e., if they were selected from the label-free proteomics study, found in literature (* Sleat et al., 2017; [#]Doll et al., 2017; ^o Sjödin et al., 2019) or from the label-free proteomics study of the urine of CLN5 and CLN6 sheep. The gene names labeled in bold were reliably detected in human urine.

9-fold relative to patients with other NCL types (CLN1, CLN3, CLN5, CLN6, and CLN7). Comparison of the levels of BHMT1, LAMP1, and TPP1 in pre-treatment and ongoing treatment (post) samples did not show any visible trend (only two paired samples available so statistical testing is not possible), although for one patient, TPP1 did increase to a measurable amount (Figure 3D), suggesting that the ERT delivered into the brain ventricles may not stay confined to the CNS. However, the other proteins in this patient did not decrease suggesting that the levels of TPP1 coming from the CNS are not at a level sufficient to correct the rest of the diseased organ systems.

ERT administered into the brain might not alter the proteins that come from the periphery, i.e., kidney lysosomes. Levels of BHMT1 have increased in Patient ID-1 with ongoing treatment, but levels of LAMP1 and TPP1 have remained constant, whereas patient ID-3 reveals a constant BHMT1 level but increasing levels for LAMP1 and TPP1 with ongoing treatment.

Proteins assessed in CLN5 and CLN6 sheep models: liver-enriched antimicrobial peptide-2 (LEAP2), desmocollin 2 (DSC2), cathepsin B (CTSB), secretagogin (SCGN), and lysosomal-associated membrane protein 2 (LAMP2) were identified as significantly altered in the sheep urine proteomic analysis and included in the targeted LC-MS/MS assay (Tables S2 and S3). CTSB and SCGN were not detectable in human urine. Figure 4A shows label-free proteomics data for increased levels of DSC2 in CLN5 and CLN6 ($p < 0.017$), increased LAMP2 in CLN5 ($p < 0.028$), and reduced LEAP2 in the CLN5 ($p < 0.01$) and CLN6 ($p < 0.003$) sheep urine. Targeted analysis (Figure 4B) of LAMP2, LEAP2, and DSC2 for CLN5 and CLN6 patients did not show a difference relative to controls.

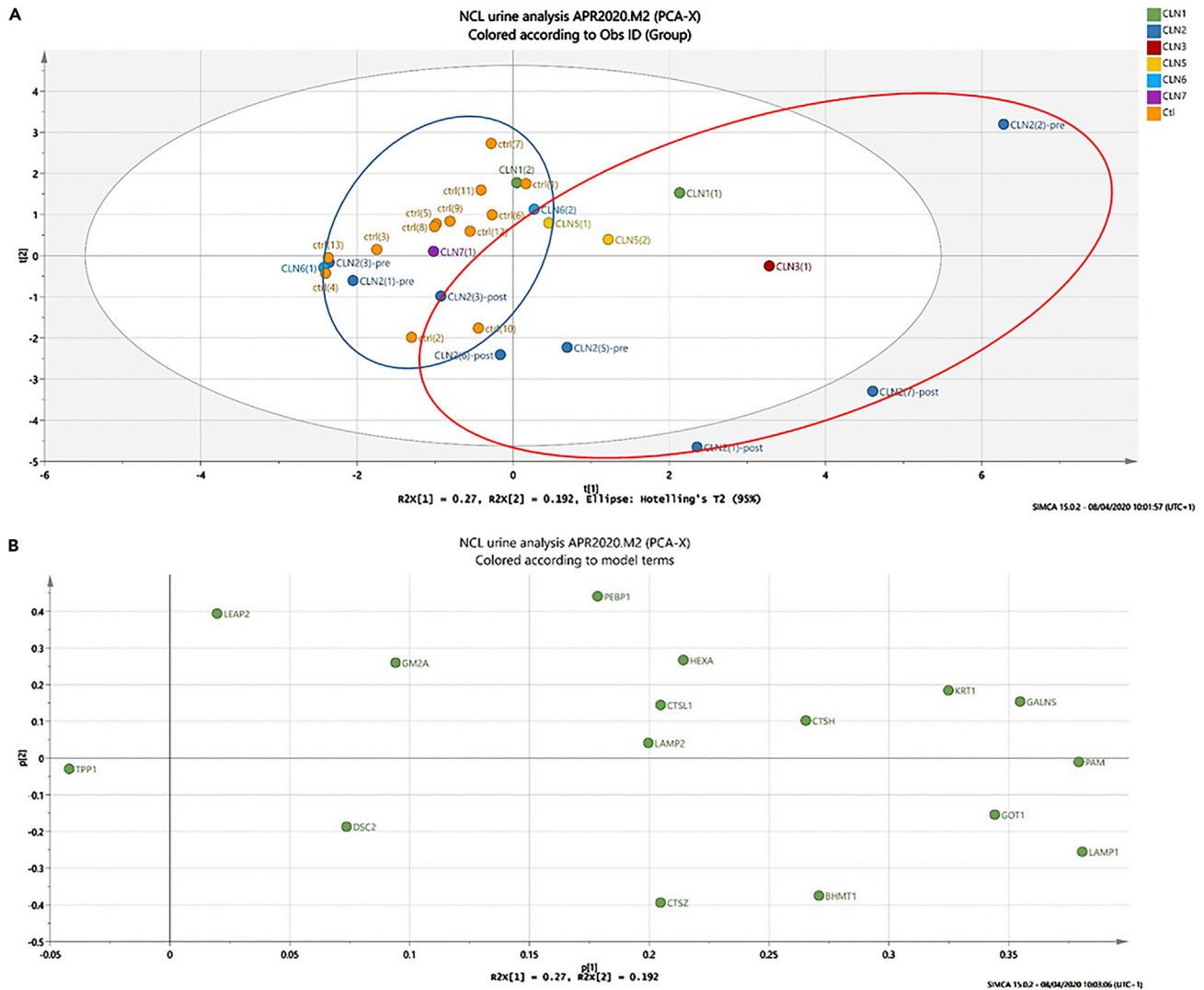


Figure 2. Multivariate analysis of targeted proteomics data of NCL patient urine

Principle-component analysis of all patient (apart from one outlier, namely, CLN2(4)-post) and control samples using SIMCA presents two almost separate clusters to distinguish between NCL and control samples.

(A and B) (A) Score plot of the samples with the control samples cluster highlighted. Samples outside the control cluster are also highlighted. (B) Loading plot of the measured proteins indicating which proteins are driving the variation/change in the score plot.

Proteins affected in NCL: [Figure 5A](#) shows the comparison of all NCL patient samples as a disease group with controls. HEXA, LAMP1, TPP1, and GOT1 are significantly altered ($p < 0.05$). LAMP1 and HEXA are increased 3-fold on average, and GOT1 is elevated 6-fold. TPP1 is reduced when compared with controls for all NCL samples. [Figure 5B](#) shows a breakdown of the NCL groups compared with each other and controls for all proteins that have shown significant change. BHMT1 is specific to CLN2 as observed previously. HEXA is increased in CLN5, CLN3, and CLN1 patients and in some patients with CLN2 and CLN6. GOT1 and LAMP1 are raised in CLN5, CLN3, and some CLN2 patients. TPP1, although the affected protein in CLN2 disease, is also reduced in all other NCL forms relative to controls. The CLN7 patient sample, as indicated in the multivariate analysis, did not show many protein changes apart from reduced TPP1.

DISCUSSION

Using an animal model and human patient samples, we have employed a two-phase proteomic discovery and validation strategy to identify and confirm urinary proteins altered in patients with NCL. Urine is an

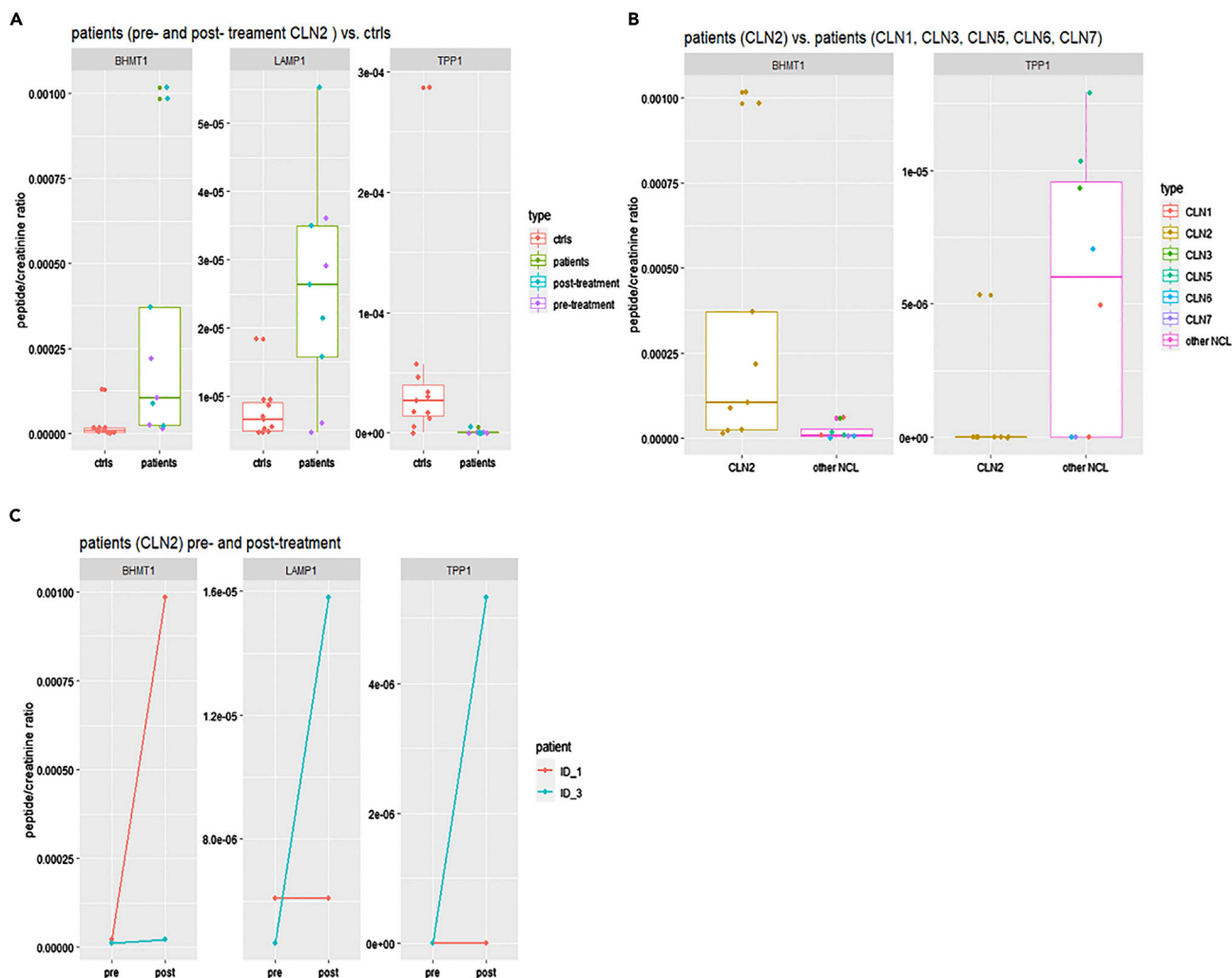


Figure 3. Targeted analysis of CLN2 patient samples

The y axis shows the amount of each protein normalized to the amount of creatinine in each sample. As the f-test showed that the variance is unequally distributed a two-sample t test assuming unequal variance was performed for each protein. For box and whisker plot: error bars are the 95% confidence interval, the bottom and top of the box are the 25th and 75th percentiles, the line inside the box is the 50th percentile (median), and any outliers are shown as open circles.

(A) Comparison of patients with CLN2 disease (color coded) with age- and sex-matched controls. The amount of LAMP1 is significantly increased in the CLN2 disease patient samples (p (two tail) = 0.010). The amount of BHMT1 shows a borderline increase in the CLN2 disease patient samples (p (two tail) = 0.05). The amount of TPP1 shows a significant decrease in the CLN2 disease patient sample (p (one-tail) = 0.040).

(B) Comparison of patients with CLN2 disease with all other patients with NCL (CLN1, CLN3, CLN5, CLN6, and CLN7). The amount of BHMT1 (p (two tail) = 0.059) shows a borderline significant increase, whereas there is a significant decrease in TPP1 (p (one tail) = 0.015) in patients with CLN2 disease.

(C) Comparison of two patients with CLN2 disease pre- and post-treatment for the three significant proteins identified in CLN2 samples compared with controls. Statistical analysis is not possible as $n = 2$.

easily accessible tissue for monitoring possible biomarkers for disease progression, and treatment and is a valuable tissue resource as the kidneys present a high proportion of mitochondria and lysosomes, both known to be affected in NCL disease.

The proteomic profiling analyses were performed on samples from two patients with CLN2 disease. Proteins observed to be altered included many proteins associated with the lysosome and is consistent with CLN2 being caused by a deficiency in a lysosomal enzyme involved in protein degradation. Other pathways also potentially affected in CLN2 urine include signaling pathways, e.g., those involved in inactivation of BAG2 signaling and inflammatory response-associated pathways. The BAG2 signaling pathway, which

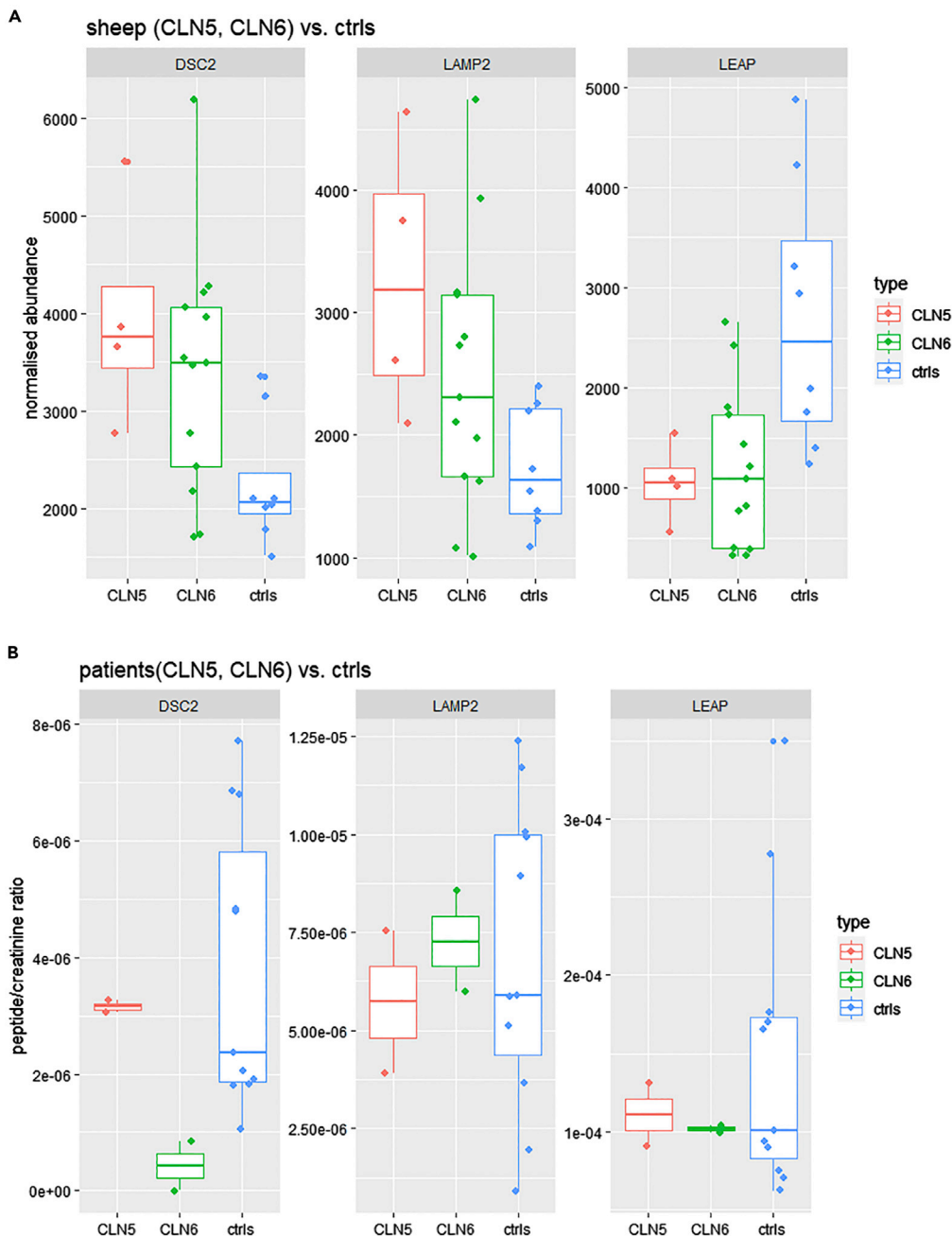


Figure 4. Evaluation in patient urine of protein biomarker candidates identified from CLN5 and CLN6 sheep models

Three proteins, DSC1, LEAP2, and LAMP2, identified in the proteomic analysis were detectable in humans. For the box and whisker plot: error bars are the 95% confidence interval, the bottom and top of the box are the 25th and 75th percentiles, the line inside the box is the 50th percentile (median), and any outliers are shown as open circles.

(A) Proteomic profiling data from the CLN5 and CLN6 sheep model analysis for these three proteins. DSC2 ($p < 0.017$) and LAMP2 ($p < 0.02$ for CLN5) were increased and LEAP2 was decreased ($p < 0.01$).

(B) Targeted analysis of these proteins in CLN5 and CLN6 patient urine. The proteins are not significantly affected in humans and DSC2 is decreased in CLN6, which is not observed in the sheep model.

includes heat shock proteins involved in the control of folding or degradation of misfolded proteins, are typically either increased or decreased in neurodegenerative disorders and implicated in the pathogenesis of various neurodegenerative diseases (Soto and Pritzkow, 2018). Many neurodegenerative diseases are

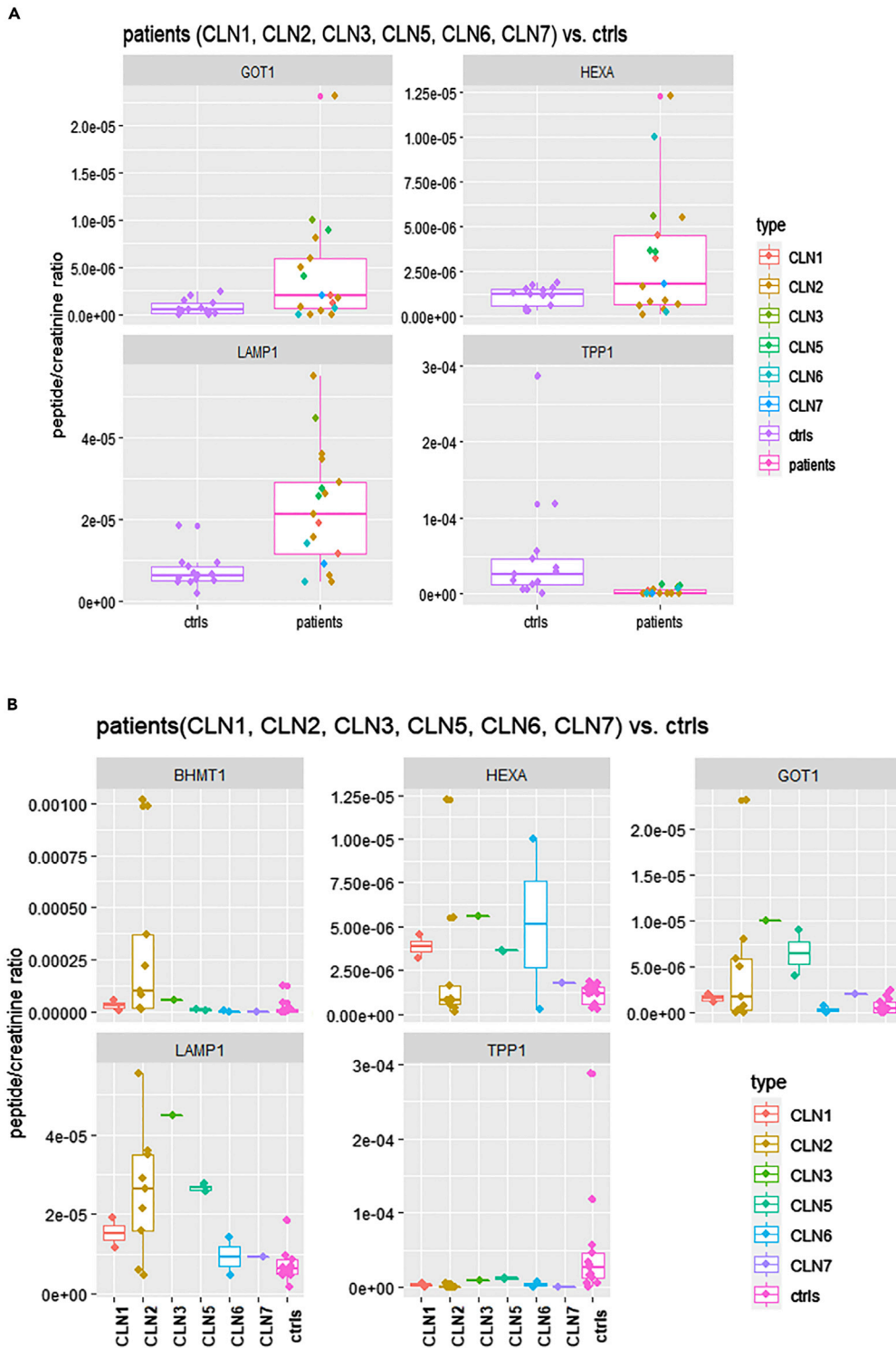


Figure 5. Proteins affected across multiple NCL forms

For the box and whisker plot: error bars are the 95% confidence interval, the bottom and top of the box are the 25th and 75th percentiles, the line inside the box is the 50th percentile (median), and any outliers are shown as open circles.

Figure 5. Continued

(A) Comparison of patients with CLN1, CLN2, CLN3, CLN5, CLN6, and CLN7 disease (color coded) with age- and sex-matched controls. The difference in the amounts of GOT1 (p (two tail) = 0.023), HEXA (p (two tail) = 0.025), and LAMP1 (p (two tail) = 0.0004) are statistically significant. The amount of TPP1 shows a significant decrease (p (one tail) = 0.024). (B) A breakdown of the NCL forms compared with controls for each of the affected protein.

primarily disorders of protein misfolding and accumulation of storage material. Protein misfolding would be expected to be affected in CLN2 disease due to the lysosomal accumulation of mitochondrial ATP-synthase subunit-c, which has been shown to be stored in lysosome-derived organelles in many but not all NCL, including CLN 2, 5, 6 diseases (Palmer, 2015; Chen et al., 2004; Palmer et al., 1989, 1992). Protein misfolding is clearly a pathological pathway in the brain and other tissues that we can observe in patient urine, and is consistent with the systemic pathology of CLN2 disease that affects nearly all cell types in the body. Other potentially affected pathways also include integrin-like kinase (ILK) signaling, which promotes cell growth. Altered cell growth has previously been described in NCL disease models (Guo et al., 1999; Huber et al., 2014; Mahmood et al., 2013; Savchenko et al., 2017; Sleat et al., 2017). Other pathways that may be affected involve inflammation reflective of neuroinflammation, which is common to the ovine diseases and several other NCLs (Palmer et al., 2013; Kay et al., 2006; Oswald et al., 2005; Nelvagal et al., 2020), that is known to occur due to stress of the ER from the unfolded protein response (Marotta et al., 2017). Proteins affected in patients with CLN2 disease included FMO3, which is likely to be present due to its role in metabolism of administered drugs. Phosphatidylethanolamine-binding protein 1 (PEBP1) is a protease inhibitor with multiple functions; why it is increased in CLN2 is unknown. GALNS N-acetylgalactosamine-6-sulfatase and beta-hexosaminidase alpha are part of the glycosaminoglycan degradation pathway, which has been previously implicated in NCL disease (Sleat et al., 2019).

Subsequent targeted analysis was performed on a larger cohort of samples from patients with CLN2 disease undergoing ERT treatment ($n = 7$, for two patients pre- and post-treatment paired samples were available) and a small number of other patients with NCL including two patients with CLN1, one with CLN3, two with CLN5, two with CLN6, and one with CLN7 disease. We compared data of the NCL disease group, involving all samples, and that of the CLN2 disease group with controls. Proteins that were found specific for CLN2 disease included BHMT1 as shown in Figures 3A and 5B. BHMT1 is a zinc-dependent cytosolic enzyme that catalyzes the transfer of a methyl group from betaine to homocysteine. This reaction results in increased dimethylglycine and methionine (Teng et al., 2011). High concentrations of BHMT may indicate higher production of the substrate homocysteine. High concentrations of homocysteine in plasma are associated with cardiovascular diseases, renal insufficiency, and cognitive impairment and usually indicate vitamin B₁₂ deficiency. Why higher BHMT1 and possibly homocysteine occur specifically in patients with CLN2 disease is unknown, but they could have potential as markers for monitoring future treatments for patients with CLN2 disease that also target the systemic disease as well as the brain.

The lack of TPP1 in the brain is known to cause neurological disease, but the deficiency of TPP1 outside the CNS could also indicate a wider functional impairment. This may be associated with the progression of cardiac pathology suggested to occur in some NCL forms, including CLN2 disease (Fukumura et al., 2012; Katz et al., 2017; Ostergaard et al., 2011). It is assumed that upon administration of ERT directly into the CSF the neurological burden is relieved, and a longer lifespan becomes possible, which may result in pathology developing in the untreated organs becoming apparent (Katz et al., 2017). Treatments that target not just the CNS will likely also be needed, and the ability to monitor urinary TPP1 could be of benefit in this scenario. Another protein significantly increased in urine of patients with CLN2 disease is LAMP1, but this is not specific to CLN2. This lysosomal-associated membrane protein is situated in a dynamic equilibrium between lysosomes, endosomes, and the plasma membrane and is partially responsible for maintaining lysosomal integrity, pH, and catabolism (Xicoy et al., 2019; Eskelinen, 2006). LAMP1 is a widely used biomarker for lysosomes and lysosomal storage disorders but is usually measured in plasma or cells (Meikle et al., 1997). The elevated levels of LAMP1 in urine of patients with NCL may indicate the higher burden on the lysosome. Other urinary proteins increased in NCL disorders include GOT1 and HEXA. HEXA is increased in most patients with NCL; however, it is not increased sufficiently in patients with CLN2 disease to be significant when compared with the corresponding controls. HEXA is part of the glycosphingolipid degradation pathway (Breiden and Sandhoff, 2020; Hepbildikler et al., 2002). Specific deficiency of HEXA results in the lysosomal storage disorder called Tay Sachs disease (Okada and O'Brien, 1969). This observation of HEXA in urine here confirms a previous study that showed that the enzymatic activity of HEXA in CSF from patients with CLN2 and CLN3 disease is significantly increased (Sleat et al., 2017).

HEXA was also found to be altered in the *Dictyostelium* NCL model of CLN3 disease, indicating this enzyme is affected across different species model systems and may be a suitable biomarker candidate. Like HEXA, CLN5 has been described to also be a glycolytic hydrolase (Huber and Mathavarajah, 2018), indicating this particular molecular function is relevant in NCL disease pathology.

The fact that HEXA is increased but most other lysosomal enzymes are not indicates that it may not derive from lysosomes of disrupted cells. The HEXA could come from mast cells as it is a known marker of mast cell degranulation (Moon et al., 2014). Mast cell activity has not been specifically assessed in NCL, but mast cells have been observed to surround the optic nerve in a mouse model for CLN3 disease indicating compromise of the blood-brain barrier (Sappington et al., 2003). Proteomic analysis of CLN1 and CLN2 mouse model brain tissue has shown increased levels of CD63 (Sleat et al., 2019), which is thought to play a role in activation of mast cells and basophils (Kabashima et al., 2018). Therefore it is possible that the presence of HEXA is indicative of a mast cell-associated immune response in NCL.

Glutamic-oxaloacetic transaminase 1 is a cytosolic enzyme that plays a role in amino acid metabolism and the urea and tricarboxylic acid cycles. In principle GOT1 is a bidirectional enzyme, which turns it into an important regulator of glutamate concentration, the major excitatory neurotransmitter of the CNS, and also of aspartic acid levels. The form seen in urine is likely derived from kidney and plasma, which itself contains GOT1 from liver and muscle. Clinically GOT1 in plasma is routinely measured as aspartate aminotransferase 1 (ALT) and is a known marker of tissue damage. Increased plasma ALT has been observed in a canine model of CLN2 disease undergoing intracerebroventricular gene therapy (Katz et al., 2017), which also noted that treated dogs went on to develop cardiac disease, which is the likely source of the raised ALT. The elevated GOT1/ALT seen in NCL is probably due to tissue damage. It is plausible that this could be from the heart as progressive cardiac disease has been reported in children and adults with NCL (Os-tergaard et al., 2011; Katz et al., 2017; Fukumura et al., 2012).

We considered the specificity of these proteins as biomarkers for NCL or Lysosomal Storage Disorders (LSDs). LAMP1 is already well documented as a general marker of lysosome dysfunction and lysosomal disease (Meikle et al., 1997). We have profiled urine from patients with mucopolysaccharidosis and Niemann Pick C disease (unpublished data, Table S9). GOT1 was not affected, but interestingly, levels of BHMT are significantly reduced in NPC patient urine, the opposite of that observed in CLN2 disease. Why this occurs is unknown, but it does indicate that methionine metabolism is perturbed in LSDs.

ALT (GOT1) and HEXA are routinely measured in the clinical setting to monitor tissue damage and mast cell degranulation, so it would be possible to include these proteins when monitoring the effect of future novel systemic treatments. In summary, we have identified BHMT1 as a new biomarker in CLN2 disease and GOT1 (ALT) for systemic NCL disease as well as the known marker LAMP1. Furthermore, although we were unable to demonstrate that biomarkers in the sheep CLN5 and CLN6 models can translate to humans, we have confirmed the involvement of HEXA as observed in previous studies on the eukaryotic model system *Dictyostelium* (Huber et al., 2014).

Limitations of the study

The scarcity of available patient samples due to these disorders being rare means it will always be difficult to ascertain statistical significance in such studies. The targeted analysis unfortunately did not confirm the proteins detected in the sheep as altered in human CLN5 and CLN6 disease samples. CTSB, alpha-N-acetylgalactosaminidase (NAGA), and RAC-alpha serine/threonine-protein kinase (AKT1) could not be detected in the human urine. Animal models can be very useful for understanding disease pathology and designing treatments, but their application to identify biomarkers in humans as in this scenario is limited so far.

Resource availability

Lead contact

Wendy E Heywood wendy.heywood@ucl.ac.uk.

Materials availability

This study did not generate new unique reagents.

Data and code availability

Original data have been deposited to PeptideAtlas at <http://www.peptideatlas.org/PASS/PASS01636>.

METHODS

All methods can be found in the accompanying [Transparent methods supplemental file](#).

SUPPLEMENTAL INFORMATION

Supplemental information can be found online at <https://doi.org/10.1016/j.isci.2020.102020>.

ACKNOWLEDGMENTS

The authors would like to thank the Batten Disease Support and Research Association (BDSRA), USA, Noah's Hope/Hope for Bridget and Drew's Hope for funding this project. Medical Research Council (Grant No MR/R025134/1) supported research (S.E.M.). All research at Great Ormond Street Hospital NHS Foundation Trust and UCL Great Ormond Street Institute of Child Health is made possible by the NIHR Great Ormond Street Hospital Biomedical Research Center. The views expressed are those of the author(s) and not necessarily those of the NHS, the NIHR, or the Department of Health. We would also like to thank Martin Wellby and Dr. Katharina Russell, Lincoln University, for collecting the ovine samples.

AUTHOR CONTRIBUTIONS

K.I. created the targeted assay, performed the targeted analysis, and wrote the manuscript. R.C. performed the sheep urine analysis. P.M. enabled provision of patient samples, study design, and concept. B.C. provided patient samples. P.G. enabled provision of patient samples, study design, and concept. S.E.M., study design and concept and expertise. D.N.P. provided sheep model samples. K.M., study design and concept and resources. W.E. H., funding, concept, study design, and wrote manuscript. All authors contributed to manuscript writing and revision.

DECLARATION OF INTERESTS

P.G. is an investigator on BioMarin-sponsored studies and has received research grants and speaker honoraria. S.E.M. receives financial support from BioMarin Pharmaceutical Inc. to maintain the NCL Mutation Database. W.E.H. has received a travel award from BioMarin Pharmaceutical Inc. The remaining authors declare no competing interests.

Received: July 24, 2020

Revised: August 11, 2020

Accepted: December 29, 2020

Published: February 19, 2021

REFERENCES

- Adams, H.R., and Mink, J.W. (2013). Neurobehavioral features and natural history of juvenile neuronal ceroid lipofuscinosis (batten disease). *J. Child Neurol.* 28, 1128–1136.
- Breiden, B., and Sandhoff, K. (2020). Mechanism of secondary ganglioside and lipid accumulation in lysosomal disease. *Int. J. Mol. Sci.* 21, 2566.
- Butz, E.S., Chandrachud, U., Mole, S.E., and Cotman, S.L. (2020). Moving towards a new era of genomics in the neuronal ceroid lipofuscinoses. *Biochim. Biophys. Acta Mol. Basis Dis.* 1866, 165571.
- Chen, R., Fearnley, I.M., Palmer, D.N., and Walker, J.E. (2004). Lysine 43 is trimethylated in subunit C from bovine mitochondrial ATP synthase and in storage bodies associated with batten disease. *J. Biol. Chem.* 279, 21883–21887.
- de Blicke, E.A., Augustine, E.F., Marshall, F.J., Adams, H., Cialone, J., Dure, L., Kwon, J.M., Newhouse, N., Rose, K., Rothberg, P.G., et al. (2013). Methodology of clinical research in rare diseases: development of a research program in juvenile neuronal ceroid lipofuscinosis (JNCL) via creation of a patient registry and collaboration with patient advocates. *Contemp. Clin. Trials* 35, 48–54.
- di Ronza, A., Bajaj, L., Sharma, J., Sanagasetti, D., Lotfi, P., Adamski, C.J., Collette, J., Palmieri, M., Amawi, A., Popp, L., et al. (2018). CLN8 is an endoplasmic reticulum cargo receptor that regulates lysosome biogenesis. *Nat. Cell Biol.* 20, 1370–1377.
- Doll, S., Dreßen, M., Geyer, P.E., Itzhak, D.N., Braun, C., Doppler, S.A., Meier, F., Deutsch, M.-A., Lahm, H., Lange, R., et al. (2017). Region and cell-type resolved quantitative proteomic map of the human heart. *Nat. Commun.* 8, 1469.
- Eskelinen, E.-L. (2006). Roles of LAMP-1 and LAMP-2 in lysosome biogenesis and autophagy. *Mol. Aspects Med.* 27, 495–502.
- Fukumura, S., Saito, Y., Saito, T., Komaki, H., Nakagawa, E., Sugai, K., Sasaki, M., Oka, A., and Takamisawa, I. (2012). Progressive conduction defects and cardiac death in late infantile neuronal ceroid lipofuscinosis. *Dev. Med. Child Neurol.* 54, 663–666.
- Golabek, A.A., Kida, E., Walus, M., Wujek, P., Mehta, P., and Wisniewski, K.E. (2003). Biosynthesis, glycosylation, and enzymatic processing in vivo of human tripeptidyl-peptidase I. *J. Biol. Chem.* 278, 7135–7145.
- Griffey, M., Macauley, S.L., Ogilvie, J.M., and Sands, M.S. (2005). AAV2-mediated ocular gene therapy for infantile neuronal ceroid lipofuscinosis. *Mol. Ther.* 12, 413–421.

- Guo, W.X., Mao, C., Obeid, L.M., and Boustany, R.M. (1999). A disrupted homologue of the human CLN3 or juvenile neuronal ceroid lipofuscinosis gene in *Saccharomyces cerevisiae*: a model to study Batten disease. *Cell Mol. Neurobiol.* 19, 671–680.
- Harpole, M., Davis, J., and Espina, V. (2016). Current state of the art for enhancing urine biomarker discovery. *Expert Rev. Proteomics* 13, 609–626.
- Henderson, M.X., Wirak, G.S., Zhang, Y.Q., Dai, F., Ginsberg, S.D., Dolzhanskaya, N., Staropoli, J.F., Nijssen, P.C., Lam, T.T., Roth, A.F., et al. (2016). Neuronal ceroid lipofuscinosis with DNAJC5/CSPalpha mutation has PPT1 pathology and exhibit aberrant protein palmitoylation. *Acta Neuropathol.* 131, 621–637.
- Hepbildikler, S.T., Sandhoff, R., Kölzer, M., Proia, R.L., and Sandhoff, K. (2002). Physiological substrates for human lysosomal β -hexosaminidase S. *J. Biol. Chem.* 277, 2562–2572.
- Hu, J., Lu, J.-Y., Wong, A.M.S., Hynan, L.S., Birnbaum, S.G., Yilmaz, D.S., Streit, B.M., Lenartowicz, E.M., Thompson, T.C.M., Cooper, J.D., and Hofmann, S.L. (2012). Intravenous high-dose enzyme replacement therapy with recombinant palmitoyl-protein thioesterase reduces visceral lysosomal storage and modestly prolongs survival in a preclinical mouse model of infantile neuronal ceroid lipofuscinosis. *Mol. Genet. Metab.* 107, 213–221.
- Huang, D.W., Sherman, B.T., and Lempicki, R.A. (2008). Bioinformatics enrichment tools: paths toward the comprehensive functional analysis of large gene lists. *Nucleic Acids Res.* 37, 1–13.
- Huang, D.W., Sherman, B.T., and Lempicki, R.A. (2009). Systematic and integrative analysis of large gene lists using DAVID bioinformatics resources. *Nat. Protoc.* 4, 44–57.
- Huber, R.J. (2020). Molecular networking in the neuronal ceroid lipofuscinoses: insights from mammalian models and the social amoeba *Dictyostelium discoideum*. *J. Biomed. Sci.* 27, 64.
- Huber, R.J., and Mathavarajah, S. (2018). Cln5 is secreted and functions as a glycoside hydrolase in *Dictyostelium*. *Cell Signal.* 42, 236–248.
- Huber, R.J., Myre, M.A., and Cotman, S.L. (2014). Loss of Cln3 function in the social amoeba *Dictyostelium discoideum* causes pleiotropic effects that are rescued by human CLN3. *PLoS One* 9, e110544.
- Kabashima, K., Nakashima, C., Nonomura, Y., Otsuka, A., Cardamone, C., Parente, R., De Feo, G., and Triggiani, M. (2018). Biomarkers for evaluation of mast cell and basophil activation. *Immunol. Rev.* 282, 114–120.
- Kalantari, S., Jafari, A., Moradpoor, R., Ghasemi, E., and Khalkhal, E. (2015). Human urine proteomics: analytical techniques and clinical applications in renal diseases. *Int. J. Proteomics* 2015, 782798.
- Katz, M.L., Coates, J.R., Sibigroth, C.M., Taylor, J.D., Carpentier, M., Young, W.M., Winingier, F.A., Kennedy, D., Vuilleminot, B.R., and O'Neill, C.A. (2014). Enzyme replacement therapy attenuates disease progression in a canine model of late-infantile neuronal ceroid lipofuscinosis (CLN2 disease). *J. Neurosci. Res.* 92, 1591–1598.
- Katz, M.L., Johnson, G.C., Leach, S.B., Williamson, B.G., Coates, J.R., Whiting, R.E.H., Vansteenkiste, D.P., and Whitney, M.S. (2017). Extraneuronal pathology in a canine model of CLN2 neuronal ceroid lipofuscinosis after intracerebroventricular gene therapy that delays neurological disease progression. *Gene Ther.* 24, 215–223.
- Kay, G.W., Palmer, D.N., Rezaie, P., and Cooper, J.D. (2006). Activation of non-neuronal cells within the prenatal developing brain of sheep with neuronal ceroid lipofuscinosis. *Brain Pathol.* 16, 110–116.
- Kohlschütter, A., Schulz, A., Bartsch, U., and Storch, S. (2019). Current and emerging treatment strategies for neuronal ceroid lipofuscinoses. *CNS Drugs* 33, 315–325.
- Liu, W., Kleine-Holthaus, S.M., Herranz-Martin, S., Aristorena, M., Mole, S.E., Smith, A.J., Ali, R.R., and Rahim, A.A. (2020). Experimental gene therapies for the NCLs. *Biochim. Biophys. Acta Mol. Basis Dis.* 1866, 165772.
- Lu, J.-Y., Nelvagal, H.R., Wang, L., Birnbaum, S.G., Cooper, J.D., and Hofmann, S.L. (2015). Intrathecal enzyme replacement therapy improves motor function and survival in a preclinical mouse model of infantile neuronal ceroid lipofuscinosis. *Mol. Genet. Metab.* 116, 98–105.
- Mahmood, F., Fu, S., Cooke, J., Wilson, S.W., Cooper, J.D., and Russell, C. (2013). A zebrafish model of CLN2 disease is deficient in tripeptidyl peptidase 1 and displays progressive neurodegeneration accompanied by a reduction in proliferation. *Brain* 136, 1488–1507.
- Marotta, D., Tinelli, E., and Mole, S.E. (2017). NCLs and ER: a stressful relationship. *Biochim. Biophys. Acta Mol. Basis Dis.* 1863, 1273–1281.
- Meikle, P.J., Brooks, D.A., Ravenscroft, E.M., Yan, M., Williams, R.E., Jaunzems, A.E., Chataway, T.K., Karageorgos, L.E., Davey, R.C., Boulter, C.D., et al. (1997). Diagnosis of lysosomal storage disorders: evaluation of lysosome-associated membrane protein LAMP-1 as a diagnostic marker. *Clin. Chem.* 43, 1325–1335.
- Mole, S.E., Anderson, G., Band, H.A., Berkovic, S.F., Cooper, J.D., Kleine Holthaus, S.M., McKay, T.R., Medina, D.L., Rahim, A.A., Schulz, A., and Smith, A.J. (2019). Clinical challenges and future therapeutic approaches for neuronal ceroid lipofuscinosis. *Lancet Neurol.* 18, 107–116.
- Mole, S.E., Michaux, G., Codlin, S., Wheeler, R.B., Sharp, J.D., and Cutler, D.F. (2004). CLN6, which is associated with a lysosomal storage disease, is an endoplasmic reticulum protein. *Exp. Cell Res.* 298, 399–406.
- Moon, T.C., Befus, A.D., and Kulka, M. (2014). Mast cell mediators: their differential release and the secretory pathways involved. *Front. Immunol.* 5, 569.
- Nelvagal, H.R., Lange, J., Takahashi, K., Tarczyk-Luk-Wells, M.A., and Cooper, J.D. (2020). Pathomechanisms in the neuronal ceroid lipofuscinoses. *Biochim. Biophys. Acta Mol. Basis Dis.* 1866, 165570.
- Okada, S., and O'Brien, J.S. (1969). Tay-Sachs disease: generalized absence of a beta-D-N-acetylhexosaminidase component. *Science* 165, 698–700.
- Ostergaard, J.R., Rasmussen, T.B., and Molgaard, H. (2011). Cardiac involvement in juvenile neuronal ceroid lipofuscinosis (Batten disease). *Neurology* 76, 1245–1251.
- Oswald, M.J., Palmer, D.N., Kay, G.W., Shemilt, S.J., Rezaie, P., and Cooper, J.D. (2005). Glial activation spreads from specific cerebral foci and precedes neurodegeneration in presymptomatic ovine neuronal ceroid lipofuscinosis (CLN6). *Neurobiol. Dis.* 20, 49–63.
- Palmer, D.N. (2015). The relevance of the storage of subunit c of ATP synthase in different forms and models of Batten disease (NCLs). *Biochim. Biophys. Acta* 1852, 2287–2291.
- Palmer, D.N., Barry, L.A., Tyynela, J., and Cooper, J.D. (2013). NCL disease mechanisms. *Biochim. Biophys. Acta* 1832, 1882–1893.
- Palmer, D.N., Fearnley, I.M., Medd, S.M., Walker, J.E., Martinus, R.D., Bayliss, S.L., Hall, N.A., Lake, B.D., Wolfe, L.S., and Jolly, R.D. (1989). Lysosomal storage of the DCCD reactive proteolipid subunit of mitochondrial ATP synthase in human and ovine ceroid lipofuscinoses. *Adv. Exp. Med. Biol.* 266, 211–222, discussion 223.
- Palmer, D.N., Fearnley, I.M., Walker, J.E., Hall, N.A., Lake, B.D., Wolfe, L.S., Haltia, M., Martinus, R.D., and Jolly, R.D. (1992). Mitochondrial ATP synthase subunit c storage in the ceroid-lipofuscinoses (Batten disease). *Am. J. Med. Genet.* 42, 561–567.
- Sappington, R.M., Pearce, D.A., and Calkins, D.J. (2003). Optic nerve degeneration in a murine model of juvenile ceroid lipofuscinosis. *Invest. Ophthalmol. Vis. Sci.* 44, 3725–3731.
- Savchenko, E., Singh, Y., Kontinen, H., Lejavova, K., Mediavilla Santos, L., Grubman, A., Karkkainen, V., Keksa-Goldsteine, V., Naumenko, N., Tavi, P., et al. (2017). Loss of Cln5 causes altered neurogenesis in a mouse model of a childhood neurodegenerative disorder. *Dis. Model. Mech.* 10, 1089–1100.
- Schulz, A., Ajayi, T., Specchio, N., de Los Reyes, E., Gissen, P., Ballon, D., Dyke, J.P., Cahan, H., Slasor, P., Jacoby, D., et al. (2018). Study of intraventricular cerliponase alfa for CLN2 disease. *N. Engl. J. Med.* 378, 1898–1907.
- Sindelar, M., Dyke, J.P., Deeb, R.S., Sondhi, D., Kaminsky, S.M., Kosofsky, B.E., Ballon, D.J., Crystal, R.G., and Gross, S.S. (2018). Untargeted metabolite profiling of cerebrospinal fluid uncovers biomarkers for severity of late infantile neuronal ceroid lipofuscinosis (CLN2, batten disease). *Sci. Rep.* 8, 15229.
- Sjödén, S., Brinkmalm, G., Öhrfelt, A., Parnetti, L., Paciotti, S., Hansson, O., Hardy, J., Blennow, K., Zetterberg, H., and Brinkmalm, A. (2019). Endo-lysosomal proteins and ubiquitin CSF concentrations in Alzheimer's and Parkinson's disease. *Alzheimers Res. Ther.* 11, 82.
- Sleat, D.E., Tannous, A., Sohar, I., Wiseman, J.A., Zheng, H., Qian, M., Zhao, C., Xin, W., Barone, R., Sims, K.B., et al. (2017). Proteomic analysis of brain and cerebrospinal fluid from the three

major forms of neuronal ceroid lipofuscinosis reveals potential biomarkers. *J. Proteome Res.* 16, 3787–3804.

Sleat, D.E., Wiseman, J.A., El-Banna, M., Zheng, H., Zhao, C., Soherwardy, A., Moore, D.F., and Lobel, P. (2019). Analysis of brain and cerebrospinal fluid from mouse models of the three major forms of neuronal ceroid lipofuscinosis reveals changes in the lysosomal proteome. *Mol. Cell Proteomics* 18, 2244–2261.

Soto, C., and Pritzkow, S. (2018). Protein misfolding, aggregation, and conformational strains in neurodegenerative diseases. *Nat. Neurosci.* 21, 1332–1340.

Staropoli, J.F., Karaa, A., Lim, E.T., Kirby, A., Elbalalesy, N., Romansky, S.G., Leydiker, K.B., Coppel, S.H., Barone, R., Xin, W., et al. (2012). A homozygous mutation in KCTD7 links neuronal

ceroid lipofuscinosis to the ubiquitin-proteasome system. *Am. J. Hum. Genet.* 91, 202–208.

Teng, Y.-W., Mehedint, M.G., Garrow, T.A., and Zeisel, S.H. (2011). Deletion of betaine-homocysteine S-methyltransferase in mice perturbs choline and 1-carbon metabolism, resulting in fatty liver and hepatocellular carcinomas. *J. Biol. Chem.* 286, 36258–36267.

Tracy, C.J., Whiting, R.E.H., Pearce, J.W., Williamson, B.G., Vansteenkiste, D.P., Gillespie, L.E., Castaner, L.J., Bryan, J.N., Coates, J.R., Jensen, C.A., and Katz, M.L. (2016). Intravitreal implantation of TPP1-transduced stem cells delays retinal degeneration in canine CLN2 neuronal ceroid lipofuscinosis. *Exp. Eye Res.* 152, 77–87.

Whiting, R.E.H., Narfström, K., Yao, G., Pearce, J.W., Coates, J.R., Castaner, L.J., Jensen, C.A., Dougherty, B.N., Vuilleminot, B.R., Kennedy, D.,

et al. (2014). Enzyme replacement therapy delays pupillary light reflex deficits in a canine model of late infantile neuronal ceroid lipofuscinosis. *Exp. Eye Res.* 125, 164–172.

Williams, R.E., and Mole, S.E. (2012). New nomenclature and classification scheme for the neuronal ceroid lipofuscinoses. *Neurology* 79, 183–191.

Wlodawer, A., Durell, S.R., Li, M., Oyama, H., Oda, K., and Dunn, B.M. (2003). A model of tripeptidyl-peptidase I (CLN2), a ubiquitous and highly conserved member of the sedolisin family of serine-carboxyl peptidases. *BMC Struct. Biol.* 3, 8.

Xicoy, H., Peñuelas, N., Vila, M., and Laguna, A. (2019). Autophagic- and lysosomal-related biomarkers for Parkinson's disease: lights and shadows. *Cells* 8, 1317.

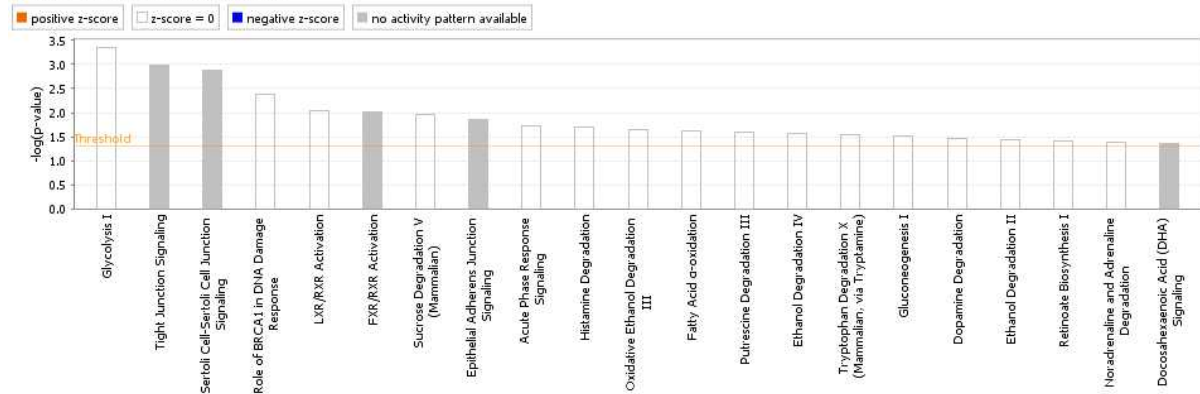
iScience, Volume 24

Supplemental Information

**Urine proteomics analysis of patients
with neuronal ceroid lipofuscinoses**

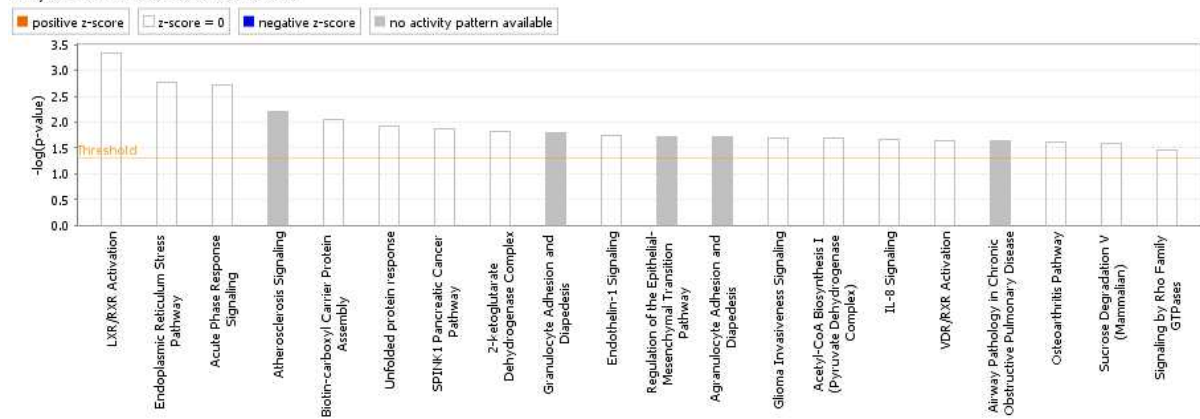
Katharina Iwan, Robert Clayton, Philippa Mills, Barbara Csanyi, Paul Gissen, Sara E. Mole, David N. Palmer, Kevin Mills, and Wendy E. Heywood

Analysis: CLN5 for IPA - 2020-05-13 08:27 AM



© 2000-2020 QIAGEN. All rights reserved.

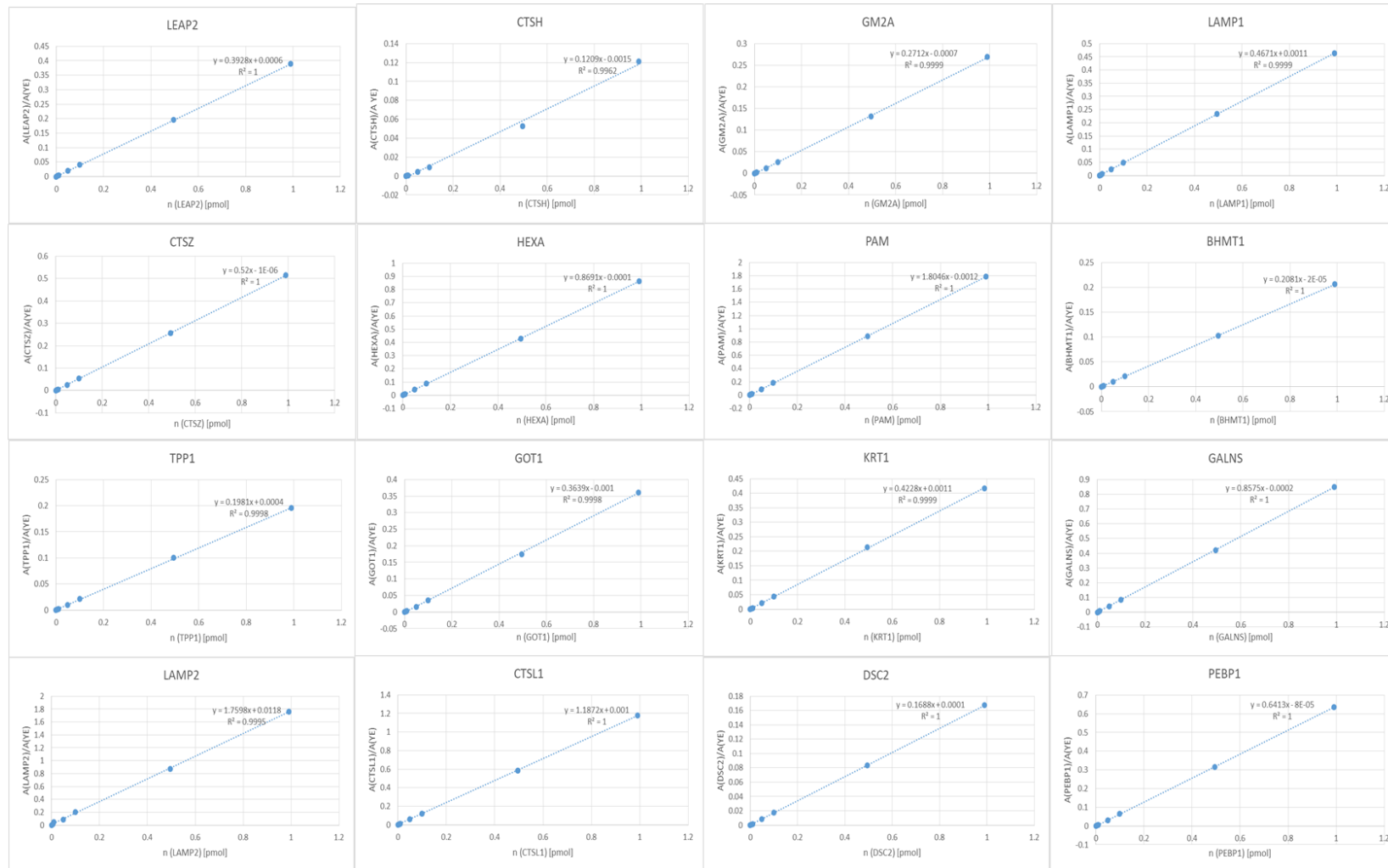
Analysis: CLN6 for IPA - 2020-05-13 08:46 AM



© 2000-2020 QIAGEN. All rights reserved.

Supplemental Figure S1: Significant pathways affected in urine CLN5 and CLN6 affected sheep Top panel IPA of CLN5. Bottom panel IPA of CLN6. Related to figure 4A.

Supplemental Figure 2: All calibration curves for the peptides of interest that were valid for quantification are shown. Related to figures 2-5



Supplemental Table S1: Untargeted proteomics analysis of 2 CLN2 vs. 4 control samples Related to figure 1.

Gene	Name	Ranking	Peptide count	Unique peptides	Confidence score	Anova (p)	fold change
GOT1	Aspartate aminotransferase, cytoplasmic	B	2	2	9.6	1.97E-05	5129.65
FMO3	Dimethylaniline monooxygenase [N-oxide-forming] 3	B	2	2	7.3	6.95E-03	2060.44
PEBP1	Phosphatidylethanolamine-binding protein 1	A	3	2	25.8	3.37E-03	69.47
GALNS	N-acetylgalactosamine-6-sulfatase	B	2	2	10.3	7.76E-04	62.99
NBPF8	Putative neuroblastoma breakpoint family member 8	B	2	2	7.8	1.19E-03	43.89
WDR19	WD repeat-containing protein 19	B	2	2	10.2	1.30E-02	27.89
BHMT	Betaine-homocysteine S-methyltransferase 1	A	7	6	58.1	1.33E-02	27.68
IGHV3-49	Protein IGHV3-49	B	2	2	13.4	1.21E-02	25.61
HEXA	Beta-hexosaminidase subunit alpha	A	7	6	32.7	1.01E-03	22.32
CTSH	Pro-cathepsin H	A	4	4	16.3	4.64E-04	20.00
HSPA1A	Heat shock 70 kDa protein 1A/1B	A	3	3	16.5	9.92E-03	18.74
CTS2	Cathepsin Z	B	2	2	9.2	4.77E-03	18.17
TPI1	Isoform 2 of Triosephosphate isomerase	A	4	3	38.6	2.04E-02	15.26
IGJ	Immunoglobulin J chain (Fragment)	A	3	3	23.4	2.13E-02	13.13
PPIA	Peptidyl-prolyl cis-trans isomerase	A	4	4	26.2	1.59E-02	12.57
ALDOB	Fructose-bisphosphate aldolase B	A	7	7	47.6	4.33E-03	11.45
COL6A1	Collagen alpha-1(VI) chain	A	17	16	133.8	2.40E-03	11.30
HSPA8	Heat shock cognate 71 kDa protein	A	6	4	37.8	1.20E-02	10.31
KRT17	Keratin, type I cytoskeletal 17	A	11	3	71.4	4.47E-03	9.94
SALL3	Sal-like protein 3 (Fragment)	B	3	3	10.9	1.88E-02	9.12
NSFL1C	NSFL1 cofactor p47	A	3	2	18.2	2.47E-02	9.12
GDF15	Growth/differentiation factor 15	A	2	2	15.7	2.69E-02	8.94
ANXA2	Annexin A2	A	9	9	53.9	1.80E-02	7.37
PRCP	Lysosomal Pro-X carboxypeptidase	A	5	5	32.4	9.95E-03	7.35
SERPINA6	Corticosteroid-binding globulin	A	4	3	30.2	4.73E-02	7.35
PECAM1	Isoform Delta14-15 of Platelet endothelial cell adhesion molecule	A	5	4	30.1	1.27E-03	7.16
LAMP1	Lysosome-associated membrane glycoprotein 1	A	5	4	35.2	7.33E-03	6.21
NAGLU	Alpha-N-acetylglucosaminidase	A	4	4	18.3	4.72E-02	6.04
SIAE	Sialate	A	5	4	29.6	2.83E-02	5.81
RECQL5	ATP-dependent DNA helicase Q5	A	7	7	23.7	4.62E-02	5.69
ICAM1	Intercellular adhesion molecule 1	A	3	3	19.2	4.87E-03	5.63
DDR1	Epithelial discoidin domain-containing receptor 1	A	4	4	20.6	4.20E-02	5.56
GUSB	Isoform 2 of Beta-glucuronidase	A	7	7	49.1	3.49E-02	5.33
ACP2	Lysosomal acid phosphatase	A	8	7	60.0	1.82E-02	5.32
IGHA2	Ig alpha-2 chain C region	B	5	1	48.9	6.69E-03	5.30
PIIB	Peptidyl-prolyl cis-trans isomerase B	B	3	3	14.6	2.11E-03	5.20
DAG1	Dystroglycan	A	4	3	31.1	1.66E-02	5.13
CSPG4	Chondroitin sulfate proteoglycan 4	A	4	2	20.4	3.95E-02	5.10
GSTP1	Glutathione S-transferase P	A	4	4	26.1	3.23E-04	4.53
SDCBP	Isoform 2 of Syntenin-1	A	6	6	36.5	1.89E-02	3.96
SOD3	Extracellular superoxide dismutase [Cu-Zn]	A	4	4	29.7	4.03E-02	3.95
GP6	Isoform 2 of Platelet glycoprotein VI	A	4	4	25.8	4.42E-02	3.72
PROZ	Vitamin K-dependent protein Z	A	9	8	76.2	1.85E-02	3.69
LCN2	Neutrophil gelatinase-associated lipocalin	A	5	5	34.3	4.12E-02	3.55
GLB1	Beta-galactosidase	A	7	7	45.6	4.90E-02	3.31
RTN4RL2	Reticulon-4 receptor-like 2	A	4	3	28.4	2.65E-03	3.18
CLEC4G	C-type lectin domain family 4 member G	A	3	2	25.0	3.35E-02	3.16
HSPA2	Heat shock-related 70 kDa protein 2	A	4	2	27.6	1.14E-02	3.13
ACTB	Actin, cytoplasmic 1	A	8	2	59.8	2.57E-03	2.78
CEACAM8	Carcinoembryonic antigen-related cell adhesion molecule 8	A	2	2	21.8	3.12E-02	2.67
TICAM2	Isoform 2 of TIR domain-containing adapter molecule 2	B	2	2	8.3	1.82E-02	2.66
ANXA5	Annexin	B	2	2	10.9	3.20E-02	2.55
CREB3L3	Cyclic AMP-responsive element-binding protein 3-like protein 3	A	3	3	17.8	4.87E-02	2.55
DLK2	Protein delta homolog 2	A	3	3	15.8	4.99E-02	2.54
ACTC1	Actin, alpha cardiac muscle 1	B	6	1	41.0	4.12E-02	2.47
EPHB2	Ephrin type-B receptor 2	A	8	7	44.6	4.75E-02	2.42
HAVCR2	Hepatitis A virus cellular receptor 2	A	8	8	78.6	8.50E-05	2.39
MMRN2	Multimerin-2	A	8	7	50.7	3.32E-02	2.33
DLST	Dihydropolyllysine-residue succinyltransferase component of 2-oxoglutarate dehydrogenase complex, mitochondrial	A	5	4	32.8	4.79E-02	2.32
KRT77	Keratin, type II cytoskeletal 1b	A	7	3	38.0	4.25E-02	2.31
SUSD2	Sushi domain-containing protein 2	A	3	3	22.9	4.95E-02	2.19
C2	Complement C2	A	7	2	40.4	1.16E-03	-2.29
FGFR1	Isoform 12 of Fibroblast growth factor receptor 1	A	4	4	17.0	1.23E-02	-2.30
CFB	Uncharacterized protein	B	6	1	35.9	1.04E-03	-2.33
DHX15	Putative pre-mRNA-splicing factor ATP-dependent RNA helicase DHX15	A	3	2	11.2	4.90E-02	-2.40
ATRX	Transcriptional regulator ATRX	A	7	6	30.3	2.16E-02	-2.56
CLSTN1	Calsyntenin-1	B	2	2	9.9	2.12E-02	-2.59
SELENBP1	Isoform 3 of Selenium-binding protein 1	A	3	3	17.2	4.15E-02	-2.78
CPQ	Carboxypeptidase Q	A	8	7	61.6	3.54E-02	-3.08
KRT19	Keratin, type I cytoskeletal 19	A	7	2	40.9	1.76E-02	-3.77
AKT1	RAC-alpha serine/threonine-protein kinase	A	3	2	22.5	1.01E-02	-4.68
FBN2	Fibrillin-2	A	7	6	43.6	1.21E-02	-36.15

Supplemental Table S2: Significant proteins from untargeted proteomics analysis of n=3 CLN5 sheep vs. = 8 control sheep urine samples (p-value (Welch test after transformation) < 0.05 and normalised fold change > 1). . Related to figure 1.

Gene	Name	Species	Ranking	Unique peptides	Confidence score	p value	fold change
ENO3	Beta-enolase	Homo sapiens	A	3	63.35	0.0178	2.3578
FANCA	Fanconi anemia group A protein	Homo sapiens	B	2	8.00	0.0155	1.7416
uncharacterised	Uncharacterized protein	Ovis aries	B	1	51.31	0.0077	1.4594
IBSP	Integrin binding sialoprotein	Ovis aries	A	5	56.62	0.0361	1.2218
RBBP8	DNA endonuclease RBBP8	Homo sapiens	A	7	42.81	0.0358	1.1808
ALDH1A1	Retinal dehydrogenase 1	Homo sapiens	A	2	19.19	0.0456	1.1206
LAMP2	Lysosomal associated membrane protein 2	Ovis aries	A	9	48.28	0.0279	1.0842
DSC2	Desmocollin 2	Ovis aries	A	7	74.71	0.0172	1.0737
CTNNA1	Catenin alpha-1	Homo sapiens	A	4	30.50	0.0478	1.0644
COX4I1	Cytochrome c oxidase subunit 4I1	Ovis aries	B	2	11.44	0.0186	1.0620
VWA3B	von Willebrand factor A domain-containing protein 3B	Homo sapiens	B	2	9.10	0.0010	1.0494
SERPINF1	Serpin family F member 1	Ovis aries	A	4	43.93	0.0156	1.0422
uncharacterised	Uncharacterized protein	Ovis aries	A	19	188.99	0.0114	-1.0398
CD93	CD93 molecule	Ovis aries	A	22	159.51	0.0415	-1.0627
ORM1	Alpha-1-acid glycoprotein	Ovis aries	A	22	143.97	0.0190	-1.0718
SCGN	Secretagoin EF-hand calcium binding protein	Ovis aries	A	2	27.50	0.0451	-1.0799
NECTIN1	Nectin cell adhesion molecule 1	Ovis aries	B	2	10.80	0.0448	-1.1338
IGSF5	Immunoglobulin superfamily member 5	Ovis aries	A	14	99.15	0.0169	-1.2003
LEAP2	Liver enriched antimicrobial peptide 2	Ovis aries	A	4	19.97	0.0102	-1.2378
NEFL	Neurofilament light polypeptide	Homo sapiens	A	6	62.09	0.0302	-1.3340

Supplemental Table S3: Significant proteins from untargeted proteomics analysis of n=13 CLN6 sheep vs. n=8 control sheep samples (p-value (Welch test after transformation) < 0.05 and normalised fold change > 1). Related to figure 1.

Gene	Name	Species	Ranking	Unique peptides	Confidence score	p value	fold change
RARRES1	Retinoic acid receptor responder 1	Ovis aries	A	2	18.14	0.0488	1.438
CTSB	Cathepsin B	Homo sapiens	A	2	36.15	0.0294	1.342
uncharacterised	Uncharacterized protein	Ovis aries	A	2	23.74	0.0110	1.230
FCGR1A	Uncharacterized protein	Ovis aries	B	2	11.20	0.0133	1.203
uncharacterised	Uncharacterized protein	Ovis aries	B	1	18.83	0.0446	1.165
CP	Ceruloplasmin	Ovis aries	A	4	23.80	0.0187	1.130
SERPINF1	Pigment epithelium-derived factor	Homo sapiens	B	1	16.98	0.0093	1.103
uncharacterised	Uncharacterized protein	Ovis aries	B	2	11.77	0.0097	1.094
CASC5	Protein CASC5	Homo sapiens	B	2	9.90	0.0487	1.076
ATP5A1	ATP synthase subunit alpha	Ovis aries	B	1	31.92	0.0362	1.064
MBTPS1	Membrane-bound transcription factor site-1 protease	Homo sapiens	B	2	10.02	0.0428	1.063
C4BPA	Complement component 4 binding protein alpha	Ovis aries	A	3	22.65	0.0039	1.057
GNAI1	Guanine nucleotide-binding protein G(i) subunit alpha-1	Homo sapiens	A	2	15.86	0.0333	1.051
DSC2	Desmocollin 2	Ovis aries	A	7	74.71	0.0164	1.049
SDC4	Syndecan	Ovis aries	A	6	35.15	0.0198	1.045
VWA3B	von Willebrand factor A domain-containing protein 3B	Homo sapiens	B	2	9.10	0.0062	1.043
APOA2	Apolipoprotein A2	Ovis aries	A	3	17.96	0.0452	1.038
PLA2G7	Platelet-activating factor acetylhydrolase	Ovis aries	A	8	69.76	0.0437	1.033
PI16	Peptidase inhibitor 16	Ovis aries	A	7	54.38	0.0367	-1.038
CATHL3	Cathelicidin-3	Ovis aries	A	6	99.46	0.0185	-1.038
QPCT	Uncharacterized protein	Ovis aries	A	14	174.09	0.0168	-1.039
uncharacterised	Uncharacterized protein	Ovis aries	A	19	188.99	0.0429	-1.041
CST6	Cystatin	Ovis aries	A	46	235.83	0.0488	-1.042
NUCB1	Nucleobindin 1	Ovis aries	A	22	196.46	0.0287	-1.060
DLAT	Acetyltransferase component of pyruvate dehydrogenase complex	Ovis aries	A	3	25.15	0.0358	-1.073
FABP4	Adipocyte fatty acid-binding protein 4	Ovis aries	A	16	146.25	0.0373	-1.077
LOC654331	Uncharacterized protein	Ovis aries	A	9	82.03	0.0311	-1.077
LOC101112304	Uncharacterized protein	Ovis aries	A	5	70.60	0.0299	-1.079
GFAP	Glial fibrillary acidic protein	Ovis aries	B	1	56.39	0.0112	-1.082
SCGN	Secretagogin_EF-hand calcium binding protein	Ovis aries	A	2	27.50	0.0097	-1.087
CUBN	Cubilin	Ovis aries	A	41	367.87	0.0467	-1.093
MMP9	Matrix metalloproteinase 9	Ovis aries	A	2	27.05	0.0285	-1.097
CALR	Calreticulin	Ovis aries	A	2	26.66	0.0112	-1.101
SH3RF1	E3 ubiquitin-protein ligase SH3RF1	Homo sapiens	A	3	36.29	0.0029	-1.108
PIGR	Polymeric immunoglobulin receptor	Ovis aries	A	51	504.29	0.0253	-1.121
ZNF420	Zinc finger protein 420	Homo sapiens	A	2	22.81	0.0039	-1.123
ACACA	Acetyl-CoA carboxylase 1	Homo sapiens	A	7	75.60	0.0409	-1.124
AKAP13	A-kinase anchor protein 13	Homo sapiens	A	12	104.23	0.0471	-1.125
uncharacterised	Uncharacterized protein	Ovis aries	A	10	139.58	0.0468	-1.139
uncharacterised	Uncharacterized protein	Ovis aries	B	1	40.51	0.0459	-1.152
RIC1	RAB6A-GEF complex partner protein 1	Homo sapiens	B	1	29.92	0.0227	-1.161
JCHAIN	Joining chain of multimeric IgA and IgM	Ovis aries	A	13	116.55	0.0373	-1.170
CHID1	Chitinase domain-containing protein 1	Homo sapiens	A	2	25.33	0.0445	-1.186
ABHD14B	Abhydrolase domain containing 14B	Ovis aries	A	2	23.87	0.0145	-1.188
uncharacterised	Lysozyme C_kidney isozyme	Ovis aries	A	25	168.46	0.0287	-1.194
TBC1D14	TBC1 domain family member 14	Homo sapiens	B	2	10.45	0.0227	-1.210
TIGIT	T-cell immunoreceptor with Ig and ITIM domains	Ovis aries	A	4	35.73	0.0042	-1.210
GSDMD	Gasdermin-D (Fragment)	Homo sapiens	B	2	9.99	0.0169	-1.215
NECTIN1	Nectin cell adhesion molecule 1	Ovis aries	B	2	10.80	0.0084	-1.215
LEAP2	Liver enriched antimicrobial peptide 2	Ovis aries	A	4	19.97	0.0032	-1.246
BGLAP	Osteocalcin	Ovis aries	A	4	48.55	0.0287	-1.282
uncharacterised	Uncharacterized protein	Ovis aries	A	6	62.69	0.0292	-1.356
DNAJB6	DnaJ homolog subfamily B member 6	Homo sapiens	B	2	10.39	0.0319	-1.417
CLIP1	CAP-Gly domain-containing linker protein 1	Homo sapiens	A	3	21.81	0.0471	-1.427
ZNF850	Zinc finger protein 850	Homo sapiens	A	3	15.71	0.0365	-1.460
uncharacterised	Uncharacterized protein	Ovis aries	B	1	25.39	0.0005	-1.537
RBMX	Uncharacterized protein	Ovis aries	A	2	16.56	0.0371	-1.547
DLST	Dihydropyridyllysine-residue succinyltransferase component of 2-oxoglutarate dehydrogenase complex_mitochondrial (Fragment)	Homo sapiens	B	1	24.78	0.0067	-1.591
TRIOBP	TRIO and F-actin-binding protein (Fragment)	Homo sapiens	A	2	16.02	0.0097	-1.597
uncharacterised	Uncharacterized protein	Ovis aries	B	2	10.00	0.0086	-1.674
DLST	Dihydropyridyllysine-residue succinyltransferase component of 2-oxoglutarate dehydrogenase complex_mitochondrial (Fragment)	Homo sapiens	B	1	66.78	0.0236	-1.705
ERICH6B	Glutamate rich 6B	Ovis aries	B	1	33.31	0.0004	-3.645

Supplemental Table S4: DAVID analysis of the target list, i.e. the significant proteins from the label-free proteomics analysis, and the background list, i.e. the non-significant proteins from the label-free proteomics analysis. Only intracellular components are listed that show a Benjamini value of < 0.05. The intracellular components highlighted in green were of interest and proteins located in that intracellular location were chosen for further targeted proteomics analysis. Related to figure 1

Intracellular Component_Target list	Count	%	PValue	List Total	Fold Enrichment	Benjamini	FDR
lysosomal lumen	8	0.076694	0.0000	70	24.50	1.82E-06	3.90E-05
sarcolemma	5	0.047934	0.0003	70	15.31	0.00736	0.368754
blood microparticle	8	0.076694	0.0000	70	13.70	7.31E-05	0.002089
melanosome	5	0.047934	0.0006	70	12.89	0.01102	0.709453
lysosome	9	0.086281	0.0000	70	10.37	6.15E-05	0.002633
membrane raft	6	0.057521	0.0011	70	7.58	0.01863	1.333783
external side of plasma membrane	6	0.057521	0.0013	70	7.33	0.01963	1.545576
focal adhesion	11	0.105455	0.0000	70	7.32	6.94E-05	0.002478
extracellular space	29	0.278017	0.0000	70	5.61	1.20E-12	1.71E-11
extracellular exosome	54	0.517688	0.0000	70	5.00	1.46E-27	1.04E-26
membrane	20	0.191736	0.0004	70	2.37	0.00826	0.472613
Intracellular Component_Background list	Count	%	PValue	List Total	Fold Enrichment	Benjamini	FDR
platelet dense granule lumen	5	1.404494	1.16E-04	352	18.49	0.001579	0.158153
platelet alpha granule lumen	19	5.337079	6.26E-18	352	17.89	3.55E-16	8.53E-15
blood microparticle	45	12.64045	1.25E-39	352	15.33	1.06E-37	1.70E-36
anchored component of external side of plasma membrane	6	1.685393	5.18E-05	352	14.12	8.00E-04	0.070507
lysosomal lumen	17	4.775281	6.02E-12	352	10.35	2.56E-10	8.19E-09
extracellular vesicle	10	2.808989	4.11E-07	352	10.35	9.32E-06	5.60E-04
extracellular matrix	41	11.51685	1.63E-22	352	7.17	1.11E-20	2.21E-19
basement membrane	10	2.808989	2.07E-05	352	6.55	3.52E-04	0.02817
melanosome	12	3.370787	3.92E-06	352	6.15	7.40E-05	0.005333
anchored component of membrane	13	3.651685	1.87E-06	352	5.96	3.73E-05	0.002541
extracellular space	150	42.13483	3.24E-76	352	5.77	5.50E-74	4.41E-73
vesicle	14	3.932584	1.16E-06	352	5.66	2.47E-05	0.00158
collagen trimer	10	2.808989	7.01E-05	352	5.63	0.001036	0.09548
external side of plasma membrane	23	6.460674	1.63E-10	352	5.59	6.17E-09	2.23E-07
extracellular exosome	280	78.65169	3.53E-161	352	5.16	1.20E-158	4.81E-158
lysosome	22	6.179775	2.97E-09	352	5.04	1.01E-07	4.05E-06
endoplasmic reticulum lumen	16	4.494382	4.92E-06	352	4.31	8.80E-05	0.006694
extracellular region	130	36.51685	3.73E-48	352	4.18	4.22E-46	5.08E-45
proteinaceous extracellular matrix	21	5.898876	2.73E-07	352	4.06	6.63E-06	3.72E-04
cell surface	41	11.51685	3.17E-13	352	3.92	1.54E-11	4.32E-10
apical plasma membrane	22	6.179775	2.40E-07	352	3.91	6.28E-06	3.27E-04
membrane raft	15	4.213483	4.82E-05	352	3.77	7.81E-04	0.065679
focal adhesion	26	7.303371	1.74E-07	352	3.44	4.94E-06	2.37E-04
integral component of plasma membrane	49	13.76404	8.76E-05	352	1.79	0.001241	0.119259
plasma membrane	126	35.39326	1.63E-08	352	1.58	5.05E-07	2.22E-05

Supplemental Table S5: Evaluation of the quality controls (QCs) made from pooled urine digests. Related to figures 3-5.

	GOT1	TPP1	LAMP2	PAM	CTSH	LEAP	GM2A	CTSZ
QC1	194.068	1.015804	0.311667	0.0409633	0.491935	5.678913	1.844095	0.611566
QC2	123.839	0.960723	0.29239	0.0353521	0.44485	5.506657	1.747883	0.558724
QC3	215.653	0.996755	0.288965	0.0511751	0.435797	5.283002	1.830296	0.588697
mean	177.8533	0.991094	0.297674	0.0424968	0.457528	5.489524	1.807425	0.586329
SD	39.19727	0.02284	0.009993	0.0065501	0.024609	0.162083	0.042478	0.021637
CV	22.0391	2.304543	3.357011	15.41308	5.378711	2.952591	2.350178	3.690281

	LAMP1	HEXA	BHMT1	KRT1	GALNS	PEBP1	DSC2	CTSL1
QC1	0.567994	0.081765	1.599123	1.8241034	0.049222	0.678218	0.189882	0.085533
QC2	0.548064	0.077686	1.598073	1.9268526	0.050182	0.700525	0.182958	0.109676
QC3	0.5466	0.084786	1.801216	1.9256295	0.05663	0.652403	0.172949	0.126183
mean	0.554219	0.081412	1.666137	1.8921951	0.052011	0.677049	0.18193	0.10713
SD	0.009759	0.002909	0.095516	0.0481507	0.00329	0.019663	0.006951	0.016693
CV	1.760781	3.573634	5.732779	2.5447016	6.324699	2.90422	3.820796	15.5816

Supplemental Table S6: Unpublished data of untargeted proteomics analyses of urine samples from ten controls and four NPC patients. Depicted are the two possible biomarkers for LSD (LAMP1) and CLN2 (BHMT1). Related to figure 3-5.

	BHMT1	LAMP1
ctrl	11.12	18.33
ctrl	9.41	17.47
ctrl	9.50	17.83
ctrl	11.93	22.06
ctrl	13.91	24.53
ctrl	12.67	23.17
ctrl	11.19	15.71
ctrl	13.05	21.27
ctrl	13.06	17.56
ctrl	13.39	12.07
NPC	10.94	18.46
NPC	9.34	12.75
NPC	6.62	21.03
NPC	6.76	13.62
mean (ctrl)	11.92	19.00
mean (NPC)	8.42	16.47
t-test	0.0049	0.2830

Transparent Methods

Ethics Approval

The collection of samples for this study has ethical approval (13/LO/0168; IRAS ID 95005; London-Bloomsbury Research Ethics Committee) and Health Research Authority (HRA) approval

Urine Samples

Table 2 lists all the urine samples used in this study. Patient samples were collected from NCL patients after obtaining informed consent and were anonymised and stored at -80 °C within 24 hours of collection. Two CLN2 patients were on cerliponase alpha treatment and pre- and post-treatment samples were obtained. The urine of 3 (3 x male) CLN5 sheep (Frugier et al., 2008) and 13 (7 female, 6 male) CLN6 sheep (Tammen et al., 2006) as well urine from 7 unaffected control sheep (2 female, 5 male) were collected and provided by Prof David Palmer Lincoln University, New Zealand from flocks maintained at Lincoln University under protocols approved by the Lincoln University Animal Ethics Committee and in accordance with the New Zealand Animal Welfare Act, 1999 and NIH guidelines. Samples were frozen at -80 °C within 24 hours of collection.

Table S7: Human cohort sample information for CLN type, age, sex and the corresponding control samples. All samples were analysed and the NCL type was determined by the Great Ormond Street Diagnostic Enzyme Laboratory. Two of the CLN2 patients are subdivided into pre- and post- which indicates whether the sample was taken pre-treatment or with ongoing ERT treatment (post). Separate patient and control samples were used in the label free proteomics discovery analysis.

patient samples	age [years]	sex
Label Free Proteomics		
CLN2a	5	M
CLN2b	7	M
4 x Control	3-10	M
Targeted Proteomics		
CLN1(1)	7.5	M
CLN1(2)	7.3	F
CLN2(1)-pre	4.3	M
CLN2(1)-post	9	M
CLN2(2)	5.7	M
CLN2(3)-pre	13.8	F
CLN2(3)-post	17.8	F
CLN2(4)	7.9	F
CLN2(5)	3	M
CLN2(6)	6.9	F
CLN2(7)	7	M
CLN3(1)	28.5	F
CLN5(1)	10.2	M
CLN5(2)	10.2	M
CLN6(1)	5.1	M
CLN6(2)	8.5	M
CLN7(1)	6.6	M
control samples		
ctrl(1)	2.4	M
ctrl(2)	5.8	F
ctrl(3)	6.2	M

ctrl(4)	6.2	M
ctrl(5)	7.2	M
ctrl(6)	9.2	F
ctrl(7)	8.5	M
ctrl(8)	12.4	F
ctrl(9)	15.4	F
ctrl(10)	16	F
ctrl(11)	31.5	F
ctrl(12)	7.5	M
ctrl(13)	11.2	M

Label Free Proteomics

Human and sheep urine was prepared as previously described. (Heywood et al., 2015) Urine samples were thawed, 2.5 mL of each sample were aliquoted into 5 mL centrifugation tubes and centrifuged for 30 min at 4600 rpm and room temperature to separate out from particulates and cell debris. 2 mL of the supernatant were filtered using an Amicon Ultra-15 filters (3 kDa). Filters were centrifuged for 60 min at 4600 rpm to desalt and concentrate the urine samples to a residual volume of approx. 200 μ L transferred to a new plastic tube and combined with the wash solution (100 μ L of 50 mM ammonium bicarbonate) of the filter. Protein was precipitated with cold acetone (800 μ L) over-night at -20 °C. Protein in acetone was centrifuged at 16900 x g for 10 min at 4 °C. The supernatant was discarded, 50 μ L of ddH₂O added to each sample, which was vortexed thoroughly and freeze-dried overnight. To each dried protein sample 20 μ L digest buffer (6M urea, 2M thioruea, 2% ASB14, 100mM Tris-HCL pH 7.8) was added and left to shake for 1 h. Next, 1.5 μ L of DTE (30 mg/mL) was added to break the disulphide bonds then samples were shaken for 1 h then 3.0 μ L of IAA added followed by shaking for another 45 min covered from light to carboamidomethylate all cysteine residues. To this solution 165 μ L of ddH₂O and 10 μ L of trypsin gold (0.1 μ g/ μ L) were added followed by incubation overnight (16 h) at 37 °C to digest the proteins.

Peptide samples underwent an SPE clean-up before LC-MS/MS analysis. Samples were diluted with 200 μ L 0.2% TFA to adjust to a final concentration of 0.1% TFA. SPE cartridges (ISOLUTE®C18, 1 mL) were equilibrated with 2 x 1 mL 70% ACN, 0.1%TFA and then 2 x 1 mL H₂O, 0.1% TFA. The samples were loaded and allow to drip by gravity, cartridges were washed with 2 x 1 mL H₂O, 0.1% TFA before the peptides were eluted in 2 x 250 μ L 70% ACN into a new plastic tubes. The solvents were evaporated, and dried peptides were stored at -20 °C until further usage. Concentrated urine was acetone precipitated and the protein pellet subjected to tryptic digestion followed by desalting using

C18 columns (Agilent, UK). Peptides were analysed over a 60-minute gradient of increasing acetonitrile using a SYNAPT G2-Si (Waters, Manchester) mass spectrometer coupled to a nanoACQUITY UPLC (Waters, Manchester) as previously described.(Bliss et al., 2016) Raw data was processed using Progenesis Qi (Nonlinear dynamics, UK) software.

Proteins were identified at first pass against a downloaded UniProt sheep reference proteome to which the sequence of P00761 porcine trypsin were added manually. Due to lack of annotation in the sheep database a second pass identification was performed using the human reference proteome database. Data was searched with fixed modifications of carboamidomethylation of cysteines, dynamic modifications of deamidation of asparagine/glutamine and oxidation of methionine, one missed cleavage sites, and a false discovery rate set at 1%. Only protein identifications with >95% confidence and more than one peptide were used to determine significance in protein expression between groups.

Statistical and bioinformatics analysis

Multivariate analysis of the targeted proteomic data was performed using SIMCA v 15 (Umetrics, Sweden). Analysis of the affected pathways was conducted with Ingenuity Pathway Analysis (IPA, Qiagen). Cellular compartment locations of proteins were analysed with DAVID Bioinformatics Resources.(Huang et al., 2008, Huang et al., 2009) Exported data were analysed using Excel and R studio. The results were depicted using R studio.

Targeted MRM LC-MS/MS Assay

Candidate selection: Proteins were selected from the label free analysis by ranking proteins by their number of detected unique peptides and their confidence score resulted in A ranked proteins with > 2 unique peptides and a confidence score > 15, B ranked proteins with either > 2 unique peptides or a confidence score > 15 and the residual proteins that were labelled as C. Only A and B ranked proteins were selected based on significance (ANOVA $p < 0.05$) and normalised fold change ($> 2, < -2$). Known lysosomal proteins observed altered in the profiling analysis were selected. Significantly decreased protein AKT1 was chosen for the targeted MRM panel since it was previously mentioned in neurodegenerative diseases, where a disruption of Akt signalling was found to contribute to the pathogenesis.(Palmieri et al., 2017). Proteins from the sheep analysis were selected based on shared significance between CLN5 and 6 which included 3 proteins (LEAP2, secretagogen and desmocollin 2). Cathepsin B and LAMP2 had a fold change greater than 2 in the analysis. Additional proteins we thought could possibly detected in urine were selected from previous published studies. Those are

proteins directly found in NCL patients (Sleat et al., 2017, Sleat et al., 2019) like Cathepsin L1 (CTSL1), TPP1 and alpha-N-acetylgalactosaminidase (NAGA) or added out of interest, i.e. PAM (Doll et al., 2017) because it was detected in a heart proteome study. Since NCLs are thought to affect other organs like the heart, this protein was added as a potential marker for heart impairment. The ganglioside GM2 activator (GM2A) was included to gain further knowledge in the ganglioside pathway.

MRM-LC-MS/MS assay development: Two representative quantotypic peptides for the human version of all proteins were identified using original label free proteomics data and the MRM database ([www.mrm/thegpm.org](http://www.mrm.thegpm.org)). The peptides of choice were custom synthesized by Genscript, USA to identify the correct m/z in urine, optimise the detection and determine the retention times. Based on the levels of detection in urine, i.e. noninterfering peaks, and reflection of quantitative values the optimal peptides per protein with two transitions each were selected. Details of those peptides are given in Supplemental Table S7 as well as calibration curves in Supplemental Figure 3.

Sample preparation: For targeted proteomic analysis urine was prepared as described above after the addition of 7.5 μL of whole yeast enolase protein (30 $\mu\text{g}/\mu\text{L}$) (Sigma UK) the internal standard during sample preparation and for quantitation.

LC-MS/MS analysis: All samples were injected onto a Waters CORTECS UPLC C18+ column (90 \AA , 1.6 μm , 3 mm x 100 mm) attached to a C18+ VanGuard precolumn (Supplemental Table S5). Multiple reaction monitoring was performed over a 12 min gradient (Supplemental Table S6) on a Waters Xevo TQ-S mass spectrometer as previously described and quantitative data acquired using the transitions given in Supplemental Table S7.

Quality control and standardisation: Calibration curves of all peptides were prepared using pooled urine and ddH₂O with the same amount of yeast enolase as in the pooled urine samples. Calibration curves were measured together with a urine pool as quality controls (QCs) (Supplemental Table S8) at the beginning, in the middle and at the end of the patient and control urine samples. Urine creatinine was measured by LC-MS for every sample to be used as normalisation factor for a better comparison of the individual urine samples. (Mills et al., 2005a)

Data processing: The areas under the curve for each peptide of interest were analysed using Waters TargetLynx software. Those areas were normalised to the areas of the yeast enolase peptide internal standard. Those ratios were translated into absolute values with the linear equation of the corresponding standard curves. The absolute values of each peptide of interest in a sample were normalised to the creatinine amounts in this sample.

(Mills et al., 2005b)

Supplemental Table S8: Table of mass spectral parameters used for analysis in this study. Related to transparent methods

column	Cortecs C18 (90 Å) Waters Corp.
length	50 mm
internal diameter	2.1 mm
particle diameter	1.6 µm
column temperature	40 °C
guard column	Cortecs C18 VanGuard Pre-column (90 Å, 1.6 µm, 2.1 mm x 5 mm)
weak wash solvent	H ₂ O, 0.1% TFA
strong wash solvent	H ₂ O:ACN:MeOH:IPA 1:1:1:1
mobile phase A	H ₂ O, 0.1% FA
mobile phase B	CAN, 0.1% FA
gradient	yes
flow rate	0.5 mL/min
injection volume	3 µL
injection mode	partial loop
autosampler temperature	10 °C
capillary voltage	2.8 kV
nebulizer gas flow	8.0 bar
source temperature	150 °C
desolvation temperature	600 °C

Supplemental Table S9 Liquid chromatography gradient parameters used in this study. Related to transparent methods

Time	Flow [mL/min]	%A	%B	Curve
0.0	0.5	97	3	Initial
0.9	0.5	97	3	6
7.8	0.5	70	30	6
8.5	0.5	30	70	6
9.5	0.5	30	70	6
10.01	0.5	97	3	1
12	0.5	97	3	1

Supplemental Table S10: Mass transition and conditions for all peptides of interest used in this study. Related to transparent methods

Gene	peptide sequence	precursor ion [m/z]	product ion [m/z]	cone energy	collision energy	fragmentation
AKT1	EAPLNNFSVAQCQLMK	611.2992 ³⁺	621.2991 ⁺	35	21	b6
AKT1	EAPLNNFSVAQCQLMK	611.2992 ³⁺	679.3266 ⁺	35	21	y5
BHMT1	ISGQEVNEAACDIAR	816.8859 ²⁺	705.3348 ⁺	35	29	y6
BHMT1	ISGQEVNEAACDIAR	816.8859 ²⁺	905.4145 ⁺	35	29	y8
BHMT1	ISGQEVNEAACDIAR	816.8859 ²⁺	1019.4575 ⁺	35	29	y9
CTSB	VMFTEDLK	491.7493 ²⁺	752.3825 ⁺	35	17	y6
CTSB	VMFTEDLK	491.7493 ²⁺	883.423 ⁺	35	17	y7
CTSB	GQDHCIESEVVAGIPR	608.6283 ³⁺	513.3144 ⁺	35	21	y5
CTSB	GQDHCIESEVVAGIPR	608.6283 ³⁺	711.4512 ⁺	35	21	y7
CTSH	TGIYSSTCHK	414.1924 ³⁺	485.2084 ²⁺	35	14	y8
CTSH	TGIYSSTCHK	414.1924 ³⁺	570.2611 ²⁺	35	14	y10
CTSH	LQTFASNWR	561.7882 ²⁺	780.3787 ⁺	35	20	y6
CTSH	LQTFASNWR	561.7882 ²⁺	881.4264 ⁺	35	20	y7
CTSL1	LYGMNEEGWR	627.7822 ²⁺	921.3883 ⁺	35	22	y7
CTSL1	LYGMNEEGWR	627.7822 ²⁺	978.4098 ⁺	35	22	y8
CTSZ	VGDYGSLSGR	505.7487 ²⁺	576.31 ⁺	35	18	y6
CTSZ	VGDYGSLSGR	505.7487 ²⁺	854.4003 ⁺	35	18	y8
DSC2	ENAEVGTTSNGYK	685.3151 ²⁺	827.3894 ⁺	35	24	y8
DSC2	ENAEVGTTSNGYK	685.3151 ²⁺	926.4578 ⁺	35	24	y9
GALNS	YYEFPINLK	658.3321 ²⁺	860.4876 ⁺	35	23	y7
GALNS	YYEFPINLK	658.3321 ²⁺	989.5302 ⁺	35	23	y8
GM2A	EGTYSLPK	447.732 ²⁺	444.2817 ⁺	35	16	y4
GM2A	EGTYSLPK	447.732 ²⁺	607.345 ⁺	35	16	y5
GOT1	HIYLLPSGR	528.3035 ²⁺	805.4567 ⁺	35	18	y7
GOT1	HIYLLPSGR	528.3035 ²⁺	918.5407 ⁺	35	18	y8
GOT1	EPESILQVLSQMEK	815.9215 ²⁺	962.4975 ⁺	35	29	y8
GOT1	EPESILQVLSQMEK	815.9215 ²⁺	1075.5816 ⁺	35	29	y9
HEXA	ISYGPDWK	483.24 ²⁺	545.2718 ⁺	35	17	y4
HEXA	ISYGPDWK	483.24 ²⁺	765.3566 ⁺	35	17	y6

KRT1	TNAENEFVTIK	633.3223 ²⁺	850.4669 ⁺	35	22	y7
KRT1	TNAENEFVTIK	633.3223 ²⁺	979.5095 ⁺	35	22	y8
LAMP1	ALQATVGNSYK	576.3064 ²⁺	768.3887 ⁺	35	20	y7
LAMP1	ALQATVGNSYK	576.3064 ²⁺	839.4258 ⁺	35	20	y8
LAMP2	IPLNDLFR	494.2847 ²⁺	664.3413 ⁺	35	17	y5
LAMP2	IPLNDLFR	494.2847 ²⁺	874.4781 ⁺	35	17	y7
LAMP2	GILTVDELLAIR	656.8954 ²⁺	829.4778 ⁺	35	23	y7
LAMP2	GILTVDELLAIR	656.8954 ²⁺	928.5462 ⁺	35	23	y8
LEAP2	DDSECITR	498.2086 ²⁺	276.1666 ⁺	35	17	y2
LEAP2	DDSECITR	498.2086 ²⁺	549.2813 ⁺	35	17	y4
NAGA	NCISEQLFMEMADR	581.9215 ³⁺	621.2661 ⁺	35	20	y5
NAGA	NCISEQLFMEMADR	581.9215 ³⁺	752.3066 ⁺	35	20	y6
NAGA	TISAQNMDILQNPLMIK	644.0094 ³⁺	715.3807 ⁺	35	22	y6
NAGA	TISAQNMDILQNPLMIK	644.0094 ³⁺	843.4757 ⁺	35	22	y7
PAM	IVQFSPSGK	481.7689 ²⁺	622.3195 ⁺	35	17	y6
PAM	IVQFSPSGK	481.7689 ²⁺	750.3781 ⁺	35	17	y7
PAM	NNLVIFHR	506.788 ²⁺	572.3303 ⁺	35	18	y4
PAM	NNLVIFHR	506.788 ²⁺	671.3988 ⁺	35	18	y5
PEBP1	LYTLVLTDPDAPSR	780.917 ²⁺	858.3952 ⁺	35	28	y8
PEBP1	LYTLVLTDPDAPSR	780.917 ²⁺	971.4792 ⁺	35	28	y9
SCGN	IFAYYDVSK	553.2819 ²⁺	448.2402 ⁺	35	19	y4
SCGN	IFAYYDVSK	553.2819 ²⁺	845.404 ⁺	35	19	y7
TPP1	LYQQHGAGLFDVTR	535.6108 ³⁺	637.3304 ²⁺	35	18	y13
TPP1	LYQQHGAGLFDVTR	535.6108 ³⁺	746.371 ⁺	35	18	y5
TPP1	LFGGNFAHQASVAR	492.2565 ³⁺	607.805 ²⁺	35	16	y12
TPP1	LFGGNFAHQASVAR	492.2565 ³⁺	768.4111 ⁺	35	16	y7
YE	GNPTVEVELTTEK	709.06 ²⁺	623.49 ²⁺	35	18	y11
YE	GNPTVEVELTTEK	709.06 ²⁺	948.68 ⁺	35	20	y8

References

- Bliss, E., Heywood, W. E., Benatti, M., Sebire, N. J., Mills, K. (2016). An optimised method for the proteomic profiling of full thickness human skin. *Biological procedures online*, *18*, 15-15.
- Doll, S., Dreßen, M., Geyer, P. E., Itzhak, D. N., Braun, C., Doppler, S. A., Meier, F., Deutsch, M.-A., Lahm, H., Lange, R., Krane, M., Mann, M. (2017). Region and cell-type resolved quantitative proteomic map of the human heart. *Nature Communications*, *8*, 1469.
- Frugier, T., Mitchell, N. L., Tammen, I., Houweling, P. J., Arthur, D. G., Kay, G. W., van Diggelen, O. P., Jolly, R. D., Palmer, D. N. (2008). A new large animal model of CLN5 neuronal ceroid lipofuscinosis in Borderdale sheep is caused by a nucleotide substitution at a consensus splice site (c.571+1G>>A) leading to excision of exon 3. *Neurobiology of Disease*, *29*, 306-315.
- Heywood, W. E., Camuzeaux, S., Doykov, I., Patel, N., Preece, R.-L., Footitt, E., Cleary, M., Clayton, P., Grunewald, S., Abulhoul, L., Chakrapani, A., Sebire, N. J., Hindmarsh, P., de Koning, T. J., Heales, S., Burke, D., Gissen, P., Mills, K. (2015). Proteomic Discovery and Development of a Multiplexed Targeted MRM-LC-MS/MS Assay for Urine Biomarkers of Extracellular Matrix Disruption in Mucopolysaccharidoses I, II, and VI. *Analytical Chemistry*, *87*, 12238-12244.
- Huang, D. W., Sherman, B. T., Lempicki, R. A. (2008). Bioinformatics enrichment tools: paths toward the comprehensive functional analysis of large gene lists. *Nucleic Acids Research*, *37*, 1-13.
- Huang, D. W., Sherman, B. T., Lempicki, R. A. (2009). Systematic and integrative analysis of large gene lists using DAVID bioinformatics resources. *Nature Protocols*, *4*, 44-57.
- Mills, K., Morris, P., Lee, P., Vellodi, A., Waldek, S., Young, E., Winchester, B. (2005a). Measurement of urinary CDH and CTH by tandem mass spectrometry in patients hemizygous and heterozygous for Fabry disease. *Journal of Inherited Metabolic Disease*, *28*, 35-48.
- Mills, K., Morris, P., Lee, P., Vellodi, A., Waldek, S., Young, E., Winchester, B. (2005b). Measurement of urinary CDH and CTH by tandem mass spectrometry in patients hemizygous and heterozygous for Fabry disease. *J Inherit Metab Dis*, *28*, 35-48.
- Palmieri, M., Pal, R., Nelvagal, H. R., Lotfi, P., Stinnett, G. R., Seymour, M. L., Chaudhury, A., Bajaj, L., Bondar, V. V., Bremner, L., Saleem, U., Tse, D. Y., Sanagasetti, D., Wu, S. M., Neilson, J. R., Pereira, F. A., Pautler, R. G., Rodney, G. G., Cooper, J. D., Sardiello, M. (2017). mTORC1-independent TFEB activation via Akt inhibition promotes cellular clearance in neurodegenerative storage diseases. *Nature Communications*, *8*, 14338.
- Sleat, D. E., Tannous, A., Sohar, I., Wiseman, J. A., Zheng, H., Qian, M., Zhao, C., Xin, W., Barone, R., Sims, K. B., Moore, D. F., Lobel, P. (2017). Proteomic Analysis of Brain and Cerebrospinal Fluid from the Three Major Forms of Neuronal Ceroid Lipofuscinosis Reveals Potential Biomarkers. *Journal of Proteome Research*, *16*, 3787-3804.
- Sleat, D. E., Wiseman, J. A., El-Banna, M., Zheng, H., Zhao, C., Soherwardy, A., Moore, D. F., Lobel, P. (2019). Analysis of Brain and Cerebrospinal Fluid from Mouse Models of the Three Major Forms of Neuronal Ceroid Lipofuscinosis Reveals Changes in the Lysosomal Proteome. *Molecular & Cellular Proteomics*, *18*, 2244-2261.
- Tammen, I., Houweling, P. J., Frugier, T., Mitchell, N. L., Kay, G. W., Cavanagh, J. A. L., Cook, R. W., Raadsma, H. W., Palmer, D. N. (2006). A missense mutation (c.184C>T) in ovine CLN6 causes neuronal ceroid lipofuscinosis in Merino sheep whereas affected South Hampshire sheep have reduced levels of CLN6 mRNA. *Biochimica et Biophysica Acta (BBA) - Molecular Basis of Disease*, *1762*, 898-905.